remote sensing

MDPI

Article

MINDED-FBA: An Automatic Remote Sensing Tool for the Estimation of Flooded and Burned Areas

Eduardo R. Oliveira [1,2], Leonardo Disperati [1,*] and Fátima L. Alves [2]

[1] Dipartimento di Scienze Fisiche, della Terra e dell'Ambiente, Università degli Studi di Siena, 53100 Siena, Italy
[2] COPING TEAM—Coastal and Ocean Planning Governance, CESAM—Centre for Environmental and Marine Studies, Department of Environment and Planning, University of Aveiro, 3810-193 Aveiro, Portugal
* Correspondence: disperati@unisi.it; Tel.: +39-0577-233736

Abstract: This paper presents the MINDED-FBA, a remote-sensing-based tool for the determination of both flooded and burned areas. The tool, freely distributed as a QGIS plugin, consists of an adaptation and development of the previously published Multi Index Image Differencing methods (MINDED and MINDED-BA). The MINDED-FBA allows the integration and combination of a wider diversity of satellite sensor datasets, now including the synthetic aperture radar (SAR), in addition to optical multispectral data. The performance of the tool is evaluated for six case studies located in Portugal, Australia, Pakistan, Italy, and the USA. The case studies were chosen for representing a wide range of conditions, such as type of hazardous event (i.e., flooding or fire), scale of application (i.e., local or regional), site specificities (e.g., climatic conditions, morphology), and available satellite data (optical multispectral and SAR). The results are compared in respect to reference delineation datasets (mostly from the Copernicus EMS). The application of the MINDED-FBA tool with SAR data is particularly effective to delineate flooding, while optical multispectral data resulted in the best performances for burned areas. Nonetheless, the combination of both types of remote sensing data (data fusion approach) also provides high correlations with the available reference datasets. The MINDED-FBA tool could represent a new near-real-time solution, capable of supporting emergency response measures.

Keywords: QGIS plugin; data fusion; floods; fire; non-supervised classification; image differencing; automatic threshold selection

Citation: Oliveira, E.R.; Disperati, L.; Alves, F.L. MINDED-FBA: An Automatic Remote Sensing Tool for the Estimation of Flooded and Burned Areas. *Remote Sens.* **2023**, *15*, 724. https://doi.org/10.3390/rs15030724

Academic Editor: Fumio Yamazaki

Received: 21 December 2022
Revised: 18 January 2023
Accepted: 19 January 2023
Published: 26 January 2023

1. Introduction

Satellite Earth observations have been widely used for the study of hazardous phenomena [1]. Both optical and microwave satellite data have proven to provide essential data about the extents of hazard events, allowing us to infer their spatio-temporal evolution and to support emergency response interventions, as well as to incorporate further prevention plans [2–4]. Optical sensors measure passive energy, which usually consists of measuring reflected sunlight, which may be acquired into multispectral (MS) bands. This means that such MS capabilities may be useful to discriminate and characterize different hazardous processes (e.g., [3,5–8]), but at the cost of being limited to daytime and cloud free conditions [9–11]. On the other hand, the same processes may be recognized by means of active microwave synthetic aperture radars (SAR) operating on longer wavelengths and acquiring backscattered energy [12,13]. Such energy may be filtered according to different polarizations, which may allow features associated with hazard processes to be highlighted [14]. Furthermore, SAR data may perform independently of sunlight and cloud coverage, which may be crucial for certain events and in certain parts of the globe (e.g., regions with all-year persistent clouds) [9,11,12].

Both optical and SAR data allow multitemporal analysis and change detection procedures to be developed by integrating and comparing images acquired at different times, for which the temporal resolution of the satellite platforms is the most relevant conditioning factor [15–19]. This temporal capability of satellite imagery is particularly relevant to analyze the spatial-temporal evolution of hazard processes, as depending on their type they may develop different temporal behaviors [20,21].

The access to hazard extent products is often provided by national or international initiatives, or event-response mechanisms [22]. One of such examples is the Copernicus Emergency Management Service (EMS) [23], which provides on-demand information for selected emergency situations that arise from natural or man-made disasters anywhere in the world. Despite their recognized efficiency in providing worldwide emergency maps, these services are still dependent on activation protocols, which may delay such processed, or only be initiated for "major" events. This means that, ideally, more customizable and readily available solutions should be useful to local authorities and the public. Such solutions could involve GIS applications to facilitate the combination of multiple Earth observation (EO) datasets, the incorporation of automatic remote sensing (RS) routines and other data processing techniques, whilst also providing expedited and accurate products. Moreover, simplified user interfaces could be more easily accessed by GIS users, without requiring an extended knowledge about the software or RS techniques. Furthermore, if they are distributed as open-source, they also allow experts to acknowledge each processing step to keep developing and adapting beyond the "black-box" tool perspective. Repositories are an extremely valuable resource provided by the GIS community which include scripts, models, and tools for several GIS platforms. In particular, QGIS plugins are a popular way of disseminating free GIS tools, which allows a reduction in the complexity and time necessary to process and produce hazard-related products (e.g., [24–26]).

This paper has the objectives of a) presenting the MINDED-FBA tool, an open-source QGIS plugin aimed at determining the extent of flooded and burned areas through unsupervised classifications of MS optical and/or SAR imagery, and b) to demonstrate its application for different case studies. The MINDED-FBA tool comprises the combination, adaptation, and further development of two previous methods by [9,27].

The structure of this paper consists of a) presenting the methodological principles of the tool and the main innovations introduced in this paper, b) the presentation of six worldwide flooding and wildfire case studies, and c) the results from the implementation of the MINDED-FBA tool, a discussion of these results, and the main conclusions.

2. Methods

The MINDED-FBA tool which is presented in this paper consists of the adaptation of two previous methods, MINDED [9] and MINDED-BA [27], to produce, respectively, flooded and burned area extent maps. These methods have been further developed and integrated as an automatic QGIS plugin tool, with the objective of distributing a new open-source multi-hazard mapping tool, which allows a reduction in complexity and processing times, while facilitating satellite imagery processing by non-RS experts. The theoretical principles of the previously published methods have been preserved, including the multi-index differencing approach, as well as the automatic threshold selection procedure. Nevertheless, besides allowing multispectral data (i.e., Landsat and Sentinel-2 products) to be incorporated, the MINDED-FBA tool also allows the input of SAR data (i.e., Sentinel-1 products). The multispectral and SAR datasets can be used independently or in combination (i.e., data fusion approach) to produce automatic extent maps for flooded or burned areas, with several levels of magnitude of change, as well as to obtain uncertainty maps based on the agreement among the several modeled indices.

The plugin is freely distributed in the QGIS repository (https://plugins.qgis.org/plugins/minded_fba). The MINDED-FBA tool has been implemented with Python language for the QGIS version 3.22 (the current stable version). The graphical user interface of the plugin is shown in Figure 1.

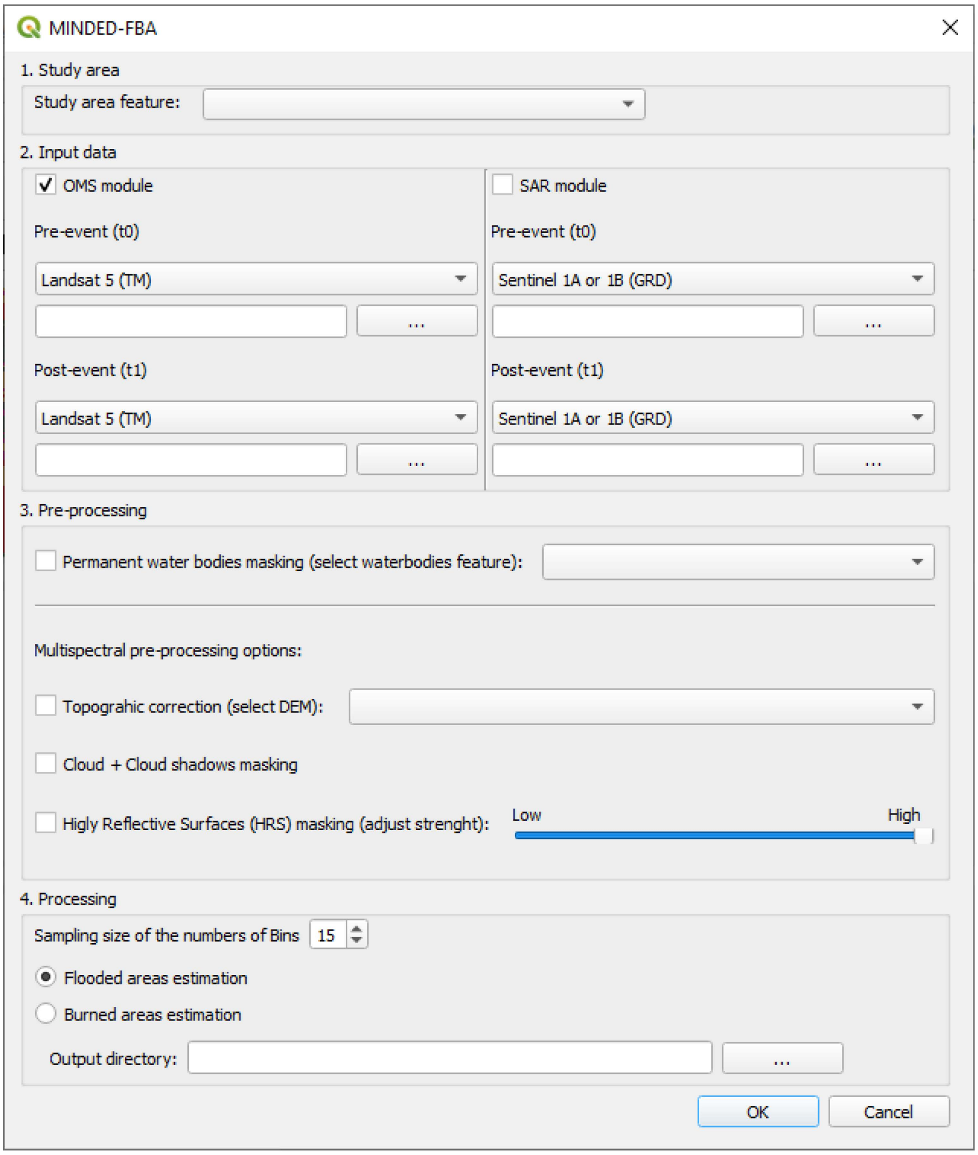

MINDED-FBA

1. Study area

Study area feature:

2. Input data

☑ OMS module

Pre-event (t0)

Landsat 5 (TM)

Post-event (t1)

Landsat 5 (TM)

☐ SAR module

Pre-event (t0)

Sentinel 1A or 1B (GRD)

Post-event (t1)

Sentinel 1A or 1B (GRD)

3. Pre-processing

☐ Permanent water bodies masking (select waterbodies feature):

Multispectral pre-processing options:

☐ Topograhic correction (select DEM):

☐ Cloud + Cloud shadows masking

☐ Higly Reflective Surfaces (HRS) masking (adjust strenght):

4. Processing

Sampling size of the numbers of Bins 15

● Flooded areas estimation

○ Burned areas estimation

Output directory:

Figure 1. The MINDED-FBA tool graphical interface.

Moreover, a detailed workflow of the MINDED-FBA procedures and outputs is represented in the Appendix A (Figure A1).

Section 1 of the MINDED-FBA tool interface includes the definition of the study area which will determine both the coordinate reference system and the processing extent of the MINDED-FBA tool procedures. The study area should be previously loaded as a QGIS layer, either vector or raster. For vector data, the MINDED-FBA automatically manages the spatial resolution of all intermediate and final products depending on the type of input data to be selected in Section 2. When using rasters, the spatial resolution of all intermediate and final products will be limited by the study area layer spatial resolution.

Section 2 "Input data" has been designed to include the folder pathways for the pre-event (*t0*) and post-event (*t1*) satellite products. The optical multispectral (OMS) module should be selected for using data acquired by passive optical sensors. In order to preserve the simplicity of the procedure and the coherence among the different available products, the tool has been designed to read specific surface reflectance data. These include the Level 2 products from the Collection 2 of the Landsat series, including Landsat 5 TM (LS5), Landsat 7 ETM+ (LS7), Landsat 8 OLI (LS8), and Landsat 9 OLI (LS9) [28–30]. Moreover, the multispectral inputs can also include Sentinel-2A (S2A) and Sentinel-2B (S2B) Level 2 products (S2MSI2A) [31]. For determining the extent of flooded areas, the MINDED-FBA tool performs automatic processing of the same indices described by [27]: NDVI, NDWI, and MNDWI. For determining the extent of burned areas, the tool processes the indices considered by [27]: NDVI, NBRs, NBRl, and NBR2. After generating single-index maps for both *t0* and *t1*, the MINDED-FBA tool proceeds with the single-index differencing, considering the same temporal order of [9] and [27] (i.e., *t1*–*t0* for flood-related data and *t0*–*t1* for burned-related data). The thematic classification of changes is determined by applying the automatic thresholding technique described by [9] and [27], which is obtained by analyzing the index-differencing distribution function (*f*), and more specifically from its first-order (*d1f*) and second-order (*d2f*) derivative functions. The technique consists of identifying the modal value of *f* in order to focus on the index-differencing values towards one of the tails of the distribution. The tail to be analyzed is simultaneously dependent on the index type, the temporal arrangement of the index differencing, and the type of change to be analyzed. Afterwards, the thresholds may be selected from either a change of sign of *d1f*, or as local maximums in *d2f* [9]. To maintain the coherence of MINDED-FBA with the previous work, we selected the two threshold values closest to the modal value (independently of them being extracted from either *d1f* or *d2f*). This means that the first threshold value (*T1*) (i.e., closer to the modal value) should correspond to the transition from the no change (Nc) condition to low-magnitude changes (LMc), while the second threshold value (*T2*) should correspond to the transition from the condition of LMc to high-magnitude changes (HMc). The thresholds are then used to perform density slicing to produce single-index change detection maps. Finally, MINDED-FBA performs a pixel-by-pixel majority analysis which combines all coeval single-index maps into one overall change detection map related to the OMS module.

Section 2 also includes a SAR module, which is one of the main innovations in comparison to the previous versions of both the MINDED and MINDED-BA [9,27]. This module allows the user to select data acquired by both Sentinel-1A and -1B sensors. The tool has been developed for incorporating Sentinel-1 products acquired in Interferometric Wide (IW) swath mode and Ground Range Detected (GRD), which consist of focused SAR data which have been detected, multi-looked, and projected to ground range using an Earth ellipsoid model [32]. GRD products are available as single or dual polarizations, with reduced speckle and approximately square resolution (at the cost of reduced spatial resolution) and pixel values represent amplitude data (phase information is discarded) [32,33]. The application of the MINDED principles to the Sentinel-1 datasets considered several combinations of polarizations (Table 1), which may be used in a similar way to multispectral indices [9,27]. However, considering the previously identified difficulties in processing and finding thresholds for non-normalized indices [9,27], we narrowed our research to normalized SAR combinations. Considering that the Normalized Ratio Procedure between Bands (NRPB) [10] and the Normalized Difference Polarization Index (NDPI) [34] are essentially additive inverses, we have narrowed the analysis to the following three SAR indices: the Normalized Ratio Procedure between Bands (NRPB) [10,35], and the Normalized Differenced Temporal Index (NDTI) for both vertical-vertical (VV) and vertical-horizontal (VH) polarizations. However, since both NDTI combinations represent bi-temporal band differencing, the single-index calculations for *t0* and *t1* are not applicable. For incorporating the above indices within the MINDED-FBA tool, we have verified if these combinations meet the same criteria introduced within the MINDED and MINDED-BA methods: (1) a modal value close to zero corresponding to the No change (Nc) condition; (2) different types of change may be located towards different sides of the frequency distribution of either the index (NDTI) or the index difference (NRPB); (3) higher magnitudes of change (further from the modal value) describing more noticeable changes; (4) change-related thresholds which may be extracted from the analysis of the frequency distribution statistics (through either the first- or second-order derivatives). Depending on the verification of these criteria and their overall performance, we may incorporate one or more SAR indices in the tool, which may be further integrated within the same majority analysis approach defined by the MINDED and MINDED-BA methods.

Table 1. Sentinel-1 indices derived from polarization combinations.

Sentinel-1 Derived Features	Equation	References
Backscattering coefficients in VH	VH	[14,35]
Backscattering coefficients in VV	VV	[14,35]
Ratio of backscattering coefficients	VH/VV	[14]
Product of backscattering coefficients	VH × VV	[14]
Difference of backscattering coefficients	VV − VH	[14]
Sum of backscattering coefficients	VV + VH	[14]
Radar Vegetation Index (RVI)	RVI = 4 × VH/(VV + VH)	[14]
Vertical Dual De-Polarization Index (VDDPI)	VDDPi = (VV + VH)/(VV)	[14]
Normalized Difference Polarization Index (NDPI)	NDPI = (VV − VH)/(VV + VH)	[34,35]
Normalized Ratio Procedure between Bands (NRPB)	NRPB = (VH − VV)/(VH + VV)	[10]
Normalized Differenced Temporal Index (NDTI) of VV	NDTI VV = (VV0 − VV1)/(VV0 + VV1)	[35]
Normalized Differenced Temporal Index (NDTI) of VH	NDTI VH = (VH0 − VH1)/(VH0 + VH1)	[35]

The OMS and SAR modules may be used separately or combined, with the latter option enabling the automatic fusion of both datasets. The MINDED-FBA tool allows the performance of both spatio-spectral (by combining both multispectral and SAR datasets) and spatio-temporal fusion (depending on the corresponding module image acquisition periods) [15,36]. Such fusion is implemented through the pixel-by-pixel majority analysis, which is applied, for every pixel, to the available indices results independently of the module. This means that whenever one of the modules does not provide outputs for a given pixel, as an effect of images extent gaps or masking procedures (see Section 3 hereunder), only the indices of the other module are used.

Section 3 corresponds to the preprocessing section, including several options for masking features which otherwise could be detected by the model as false-positives. These include the masking of permanent waterbodies, which may significantly improve the performance of the tool for the accurate detection of both flooded and burned areas, when using either the OMS or SAR modules. The masks of permanent water bodies may be based on available thematic data, which may be provided by the user as vector or raster files. Such files should be prepared in such way that those areas to be analyzed by the MINDED-FBA tool are assigned a value of 1, while those areas to be masked (i.e., corresponding to the permanent water bodies) are classified as NoData. The remaining preprocessing options included within the MINDED-FBA tool are exclusive to the OMS module. The “Cloud + Cloud shadows masking” option is available for all the previously mentioned multispectral level 2 data (including Landsat and Sentinel-2 sensors), and it is performed automatically using the respective quality bands provided with these products. The “Highly Reflective Surfaces (HRS) masking” is also available and it is particularly relevant for the detection of burned areas. It translates the procedure described by [27] and allows for the determination and implementation of sensor-specific masks, according to an *a priori* procedure of reflectance thresholding, which has been translated into a sliding bar (from high to low, with high corresponding to larger masking areas). The final preprocessing option corresponds to the “Topographic correction”, which is applied to both t0 and t1 scenes. This option performs simultaneous masking of topographic shadows and surface reflection illumination corrections (using the Cosine method) [37,38]. The procedure requires the input of a raster with elevation data, which may correspond to any digital elevation model (e.g., ALOS, SRTM).

Section 4 starts with the selection of the sampling size of the numbers of bins (equally spaced in a base 10 logarithmic scale) to be used for the statistical analysis of the frequency distribution of the index differencing. This procedure, fully described in [27], accounts for the effects of data binning on the signal-to-noise ratio characterizing the frequency distribution. This in turn influences the quality of the change-related thresholds. The default value of the sampling size (i.e., 15), as considered in previous analyses [27], may be adjusted by the user, with the software requiring longer processing times for larger values. The final section also allows the user to select the type of events to be determined (i.e., either "Flood areas estimation" or "Burned areas estimation"), which in principle should be mutually exclusive within short time periods. Lastly, the user is required to select the output folder, which will allocate all intermediate and final outputs, including statistics and raster files. The output folder will contain every coeval single-index differencing map, single-index statistics, the coeval single-index thematic maps, the overall change detection map, and the uncertainty maps. The uncertainty maps are also based on the majority analysis among all indices. The considered criteria is based on [27], with the uncertainty values ranging from lowest to highest uncertainty from 0 to 3: 0—unanimity (identical coeval classifications), 1—absolute majority, 2—relative majority, 3—no majority (tie among different coeval classifications). This analysis is performed pixel-by-pixel, taking into account the available results from either the OMS module, the SAR module, or both.

3. Study Sites and Reference Observed Event Data

The implementation of the MINDED-FBA tool plugin is demonstrated in this paper with six case studies distributed around the globe (Figure 2). The selection of these case studies prioritized the maximization of their diversity, by including three flood events and three wildfire events. They are characterized by having different scales (from local to regional events), different types of landcover and vegetation involved, bio-geographic climate regions, and morphology. For each one of these events, we could find previous assessments about their extents, which have been considered as the Reference Observed Event (ROE) dataset, for validating the MINDED-FBA tool results.

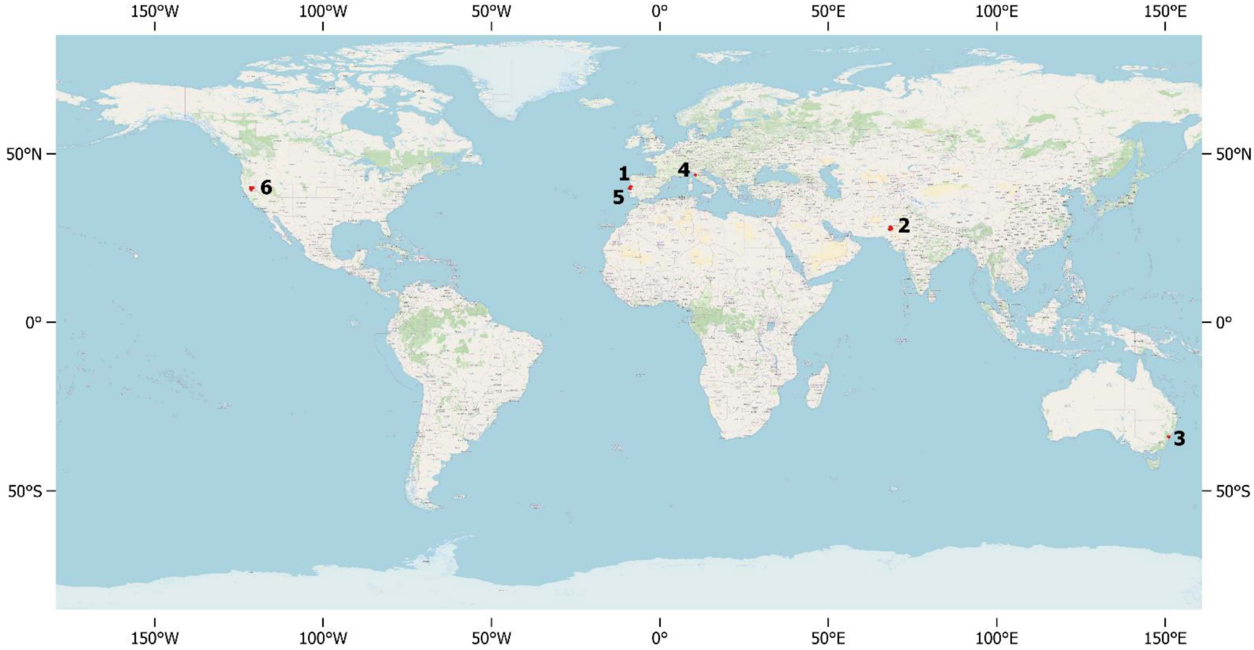

Figure 2. Location of study areas used for demonstrating the MINDED-FBA tool: (**1**) Mondego flood (Central Region, Portugal); (**2**) Sindh Province floods (Pakistan); (**3**) Richmond flood (New South Wales State, Australia); (**4**) Monte Pisano fire (Tuscany Region, Italy); (**5**) Leiria National Forest fire (Central Region, Portugal); (**6**) North-Complex fire (California State, USA) (Coordinate Reference System: WGS84/Pseudo-Mercator).

3.1. Mondego Flood (Central Region, Portugal—2019)

The first case study corresponds to the flood caused by three consecutive North Atlantic extratropical cyclones that occurred during December 2019 in the lower Mondego River (northwest-central Portugal). During the winter of 2019–2020, the cyclones named Daniel, Elsa, and Fabien swept through Portugal mainland in 16, 19, and 21 December, respectively, causing massive damages and losses, including fatalities [39]. The Coimbra district, located in the central region of Portugal's mainland, was one of the most affected areas, suffering strong winds and heavy precipitation, leading to flooded rivers and a dike breach in the lower Mondego basin.

The extent of flooding has been reported by the Copernicus EMS, which delineated the flood situation on 23 December 2019 [40]. The delineation maps used as the ROE dataset were obtained with a semi-automatic extraction, using an S2A image (acquired on 22 October 2019), and an S1A image (from 23 December 2019).

3.2. Sindh Province Floods (Southeastern Region, Pakistan—2022)

The 2022 monsoon season in Pakistan has produced abnormal rainfall since mid-June, nearly ten times higher than usual [41]. According to the National Disaster Management Authority, as of the 26 August 2022, ca. 4.25 million people have been directly affected by the floods, including the Balochistan, Sindh, Gilgit-Baltistan, Punjab, Azad Jammu and Kashmir, and Khyber Pakhtunkhwa provinces.

The Copernicus EMS service was activated on 29 August 2022, providing flood delineation maps for the Sindh Province in three areas of interest: Shikarpur, Jacobabad, and Larkana (EMSR629). These delineation maps were used as the ROE dataset and have been described to be based on pre-event images from Sentinel-2A/B (acquired on 24 March 2022) and post-event images from both SPOT6/7 (acquired on 30 August 2022) and Landsat 9 (acquired on 28 August 2022).

3.3. Richmond Flood, Australia (New South Wales State, Australia—2022)

In early 2022, as a consequence of the La Niña current, Australia experienced continuous rainfalls which resulted in numerous flood events throughout the continent. Southeastern Queensland, Wide Bay–Burnett, and parts of New South Wales were among the most affected, leading to numerous flood warnings and evacuations [42]. Multiple regions were devastated, and some of them experienced the highest flood levels in recorded history [43]. On 03 March 2022, thousands of people were evacuated within the Sydney region, and some of the most affected areas, including Richmond and Windsor, along the Hawkesbury River, were threatened by a peak spill from the Warragamba Dam.

The event resulted in the activation of the Copernicus EMS rapid mapping (EMSR567). Given the wide extent of this event, the maps were divided into 16 areas of interest (AOI), including the Richmond area (AOI 13) which was one of the largest. The thematic map considered as the ROE dataset was derived from visual interpretation of a Sentinel-2A image acquired on 11 September 2021 and a COSMO-SkyMed post-event image acquired on 03 March 2022.

3.4. Monte Pisano Fire (Tuscany Region, Italy—2018)

At the end of the summer of 2018, a large fire affected the Tuscany region (within the Pisa province). Strong winds and dry weather conditions were favorable for fire ignition and spreading, so the event reached several towns and villages. More than 700 people were temporarily evacuated due to smoke. The fire took place in Monte Pisano, a mountain system with up to 917 m elevation, burning about 10 ha of vegetation, 605 ha of olive groves, and about 40% of woodlands [44].

The Copernicus EMS was activated by the National Ministry Council—Department of Civil protection (*Presidenza del Consiglio dei Ministri—Dipartimento della Protezione Civile—Centro Situazioni* [45]), with the delineation map used as the ROE dataset reporting the situation as of 28 September 2018. The delineation is based on a pre-event image from

Sentinel-2B (acquired on 21 September 2018) and two post-event images acquired by the Pléiades-1A (from 28 September 2018) and Sentinel-2A (acquired in 26 September 2018).

3.5. Leiria National Forest Fire (Central Region, Portugal—2017)

The occurrence of fires in Mediterranean regions has been increasing as a combination of climate factors, rural abandonment, and large-scale forestation programs [26]. During the summer of 2017, Spain and Portugal had suffered a record number of devastating fires, aggravated by months of severe drought and an unusually prolonged wildfire season, with strong winds and high temperatures resulting from ex-hurricane Ophelia [46]. On 15 October 2017, numerous wildfire death casualties were reported, with evacuations taking place in several towns and villages. Marinha Grande was one of the most affected regions, with hundreds of fires devastating the Leiria National Forest (Mata Nacional de Leiria), also known as "King's Pine Forest", the largest and oldest Portuguese public forest [47].

The Copernicus EMS was activated by the National Authority for Emergency and Civil Protection on October 16 [48], resulting in the delineation map of the affected area by 17 October 2017 (AOI 01), used as the ROE dataset, based on a Sentinel-2B pre-event image (from 27 September 2017), and a post-event image from SPOT7 (from 17 October 2017).

3.6. North Complex Fire (California State, United States—2020)

The wildfire season of 2020 was a record-setting year for wildfires in California, registering nearly 10,000 fires and a total burned area with over 1.7 million hectares, being considered the largest wildfire season recorded in California's modern history [49].

The Claremont and Bear Fire, also referred to as the North Complex fire, was a large wildfire event which took place in the counties of Plumas and Butte, in California state on 17 August 2020 having been started by lightning and only becoming 100% contained on 03 December 2020. Through this period, the containment of the fire proved to be very problematic due to the steep terrain, limited road access, and several wind events with changes of direction, leading the fire to expand at catastrophic rates beyond the contingency lines. Overall, the reported burned area is of over 129 thousand hectares [50]. Thousands of hectares of timber were burned, together with loss of property, ecological damages, and the occurrence of fatalities.

The delineation used as the ROE dataset corresponds to the CAL FIRE Wildfire Perimeters and Prescribed Burns [51], which includes the entire burned area of 2020, including the North Complex fire, as well as other smaller nearby fires during that year.

4. Implementation of the MINDED-FBA Tool

4.1. Input Images Selection

For implementing the MINDED-FBA tool within the chosen study sites, we searched for available scenes to be processed with both the OMS and SAR modules. For this task, we used the USGS EarthExplorer portal [52] to find Landsat Collection 2 Level 2 products, and the Copernicus Open Access Hub [53] to search both Sentinel-2 Level 2 products (S2MSI2A) and Sentinel-1 products (GRD). For the selection of scenes, we privileged those with acquisition dates as close as possible to those considered by the ROE datasets. For the OMS module, we focused on obtaining cloud-free images. For the SAR module, we tried to find pre- and post-event images acquired with coherent acquisition modes, i.e., ascending or descending. Moreover, when analyzing mountainous areas with SAR, we tried to match the acquisition mode according to the event areas predominant slope facing orientation (i.e., ascending for south-to-west aspects, and descending for north-to-east aspects).

Table 2 summarizes the selected satellite images used for implementing the MINDED-FBA tool, including both multispectral and SAR images, alongside the ROE dataset post-event date.

Table 2. Pre- (*t0*) and post-event (*t1*) scenes processed with the OMS and SAR modules of the MINDED-FBA tool, for every case study event, alongside with the Reference Observed Event (ROE) dataset *t1* date and the study area feature processing extent (SAFPE).

Event	**OMS**		**SAR**		**ROE Dataset**	**SAFPE**
	t0	***t1***	***t0***	***t1***	***t1***	**(ha)**
1. Mondego flood	S2A 22 October 2019	S2B 29 December 2019	S1B 12 December 2019	S1A 23 December 2019	23 December 2019	147.608
2. Sindh Province floods	LS9 9 June 2022	LS8 5 September 2022	S1A 23 June 2022	S1A 3 September 2022	26 August 2022	289.057
3. Richmond flood	-	-	S1A 26 February 2022	S1A 10 March 2022	9 March 2022	91.894
4. Monte Pisano fire	S2B 21 September 2018	S2A 26 September 2018	S1A 15 September 2018	S1A 27 September 2018	26 September 2018; 28 September 2018	8.673
5. Leiria National Forest fire	LS8 5 October 2017	LS8 6 November 2017	S1A 10 October 2017	S1A 22 October 2017	17 October 2017	173.145
6. North Complex fire	LS8 26 October 2019	LS8 29 November 2020	S1B 6 December 2019	S1B 12 December 2020	31 December 2020 (*)	711.794

For the Mondego floods, we considered a couple of Sentinel-2 scenes to be used with the OMS module (S2A and S2B), and another couple of Sentinel-1 scenes (S1A and S1B) for the SAR module (Table 2). The post-event S2B scene considered in the OMS module was acquired 3 days after the post-event S1A scene of the SAR module (which was also considered by the EMS for determining the ROE dataset).

Regarding the Richmond floods, given the persistent cloud cover in the region during the period around the event, it was not possible to acquire cloud-free multispectral images. For this reason, the MINDED-FBA tool was implemented with the SAR module alone, using a couple of S1A scenes acquired in ascending mode. In particular, the post-event scene was acquired 7 days after the scene used for determining the ROE dataset.

For the Leiria National Forest fire, we considered a couple of Landsat 8 scenes for the OMS module, with a post-event image being acquired 20 days after the ROE dataset. For the SAR module, we used a couple of S1A images acquired in descending mode, acquired 3 days after the ROE dataset.

For the Monte Pisano fire, we considered the same pre-event and post-event Sentinel-2 scenes used to obtain the ROE. The multispectral data processing was performed in parallel with a couple of Sentinel-1 scenes. Considering that most of the fire took place in the south-facing slopes of this mountainous system, both selected SAR images were obtained in ascending mode.

Given the almost four-month duration of the North Complex fire, for implementing the MINDED-FBA tool we decided to analyze the entire fire season of 2020. To this aim, we considered a couple of LS8 scenes, with the pre-event image being acquired in the previous year (26 October 2019) and the post-event image acquired three days before the fire was officially declared 100% contained (29 November 2020). As for the SAR module, we considered a couple of S1B scenes, acquired in ascending mode, with the pre-event image being acquired in 6 December 2019 and the post-event image in 12 December 2020 (*).

4.2. Preprocessing Approaches and Supporting Data

In order to ensure the best accuracy of results, for this paper we considered the implementation of the MINDED-FBA tool with every available preprocessing option, as described in Chapter 2.

The option for masking permanent water bodies was selected for every case study. For those with the ROE datasets corresponding to Copernicus EMS products, we considered the polygonal hydrography features provided with the vectorial data package. As for the North Complex fire, the water mask was created with the US Census Bureau's 2016 MAF/TIGER, together with the database NHS major rivers, creeks, lakes, and reservoirs (considering a buffer of 30m around line features).

The remaining preprocessing options integrated in the MINDED-FBA tool are exclusive to the OMS module and were selected whenever that module was used (i.e., every case study, except for the Richmond flood). The "topographic correction" was implemented using the corresponding tiles from the ALOS World 3D—30m (AW3D30) database (available at [54]). For the two largest case study areas (i.e., the North Complex fire and the Sindh Province floods) we had to perform patching of several tiles of AW3D30 to include the entire extent. The "Cloud and Cloud Shadow masking" and "Highly Reflective Surfaces (HRS) masking" were also selected when using the OMS module. For the latter, we considered the highest strength of the HRS masking options (i.e., less conservative approach).

As for the SAR module, the current version of the MINDED-FBA tool does not include any further integrated preprocessing options besides the permanent waterbodies masking. Despite it being possible to directly use the Sentinel-1 GRD products, additional preprocessing procedures are strongly recommended. For every case study, we used ESA's open-source Sentinel Application Platform (SNAP) software (available at [55]) to perform a series of additional preprocessing steps on the data to be used as inputs in the SAR module. The procedures implemented in SNAP were based on [9,33] and included: i) the Orbit File Operator (with Sentinel Precise—Auto Download Orbit State Vectors); ii) the Multilook Operator; iii) Single Product Speckle Filter (Lee Sigma 7x7); and iv) Range-Doppler Terrain Correction (SRTM 3arc-sec Auto Download and Bilinear Interpolation).

4.3. Results

After gathering and preparing all the data required by the MINDED-FBA tool, as well as selecting the preprocessing options, as described in Chapter 4, we ran the tool for each case study. The following sections summarize the main results for each study area, with particular emphasis on the SAR module, which is in one of the main innovations introduced in this paper.

4.3.1. Index Calculation and Differencing

The results of the three SAR indices are illustrated in Figures 3–8, in which they are compared with the ROE delimitations of every case study. In Figures 3–5, we can verify that flood-related changes are detected by all SAR index differences as negative values, with dNRPB having an apparent reduced signal in comparison to both NDTI polarizations, which have similar results for either the VV or VH polarizations. As for the wildfire case studies, in Figures 6–8, we verify that burned-related changes also seem to be detected as negative values for every index. This means that considering the before-mentioned reversed order between pre- and post-event images, in practice they produce inverse responses along the index differencing axis. Nevertheless, in comparison to the flood-related results (Figures 3–5), the signal of burned-related changes is less evident, particularly for dNRPB, for which change-related areas are barely visible. Furthermore, for burned areas, the NDTI results seem to be more distinct between both polarizations, with burned-related changes being more evident for VV bands.

4.3.2. Binning and Thresholding

Tables 3 and 4 list the optimal bin number values, respectively, for flood and burned case study events, which were determined according to the procedure described by [27]. With the exception of the Mondego flood case study, we could not observe any significant differences in terms of the optimal bin numbers between the OMS and SAR indices.

The following step consists of determining the thresholds from either the *d1f* or *d2f*. For the OMS indices, the tool proceeds according to [9] (for floodings) and [27] (for burned areas). Regarding the SAR module, since we considered an inverse order of images in the temporal differences of floods and burned areas, for dNRPB, NDPI VV, and NDPI VH the threshold selection analysis only accounts for values smaller than the modal value of frequency distribution function (i.e., focusing only on the left tail of the *d1f* and *d2f* distributions). Tables 5 and 6 include all thresholds T1 and T2 (if applicable) found for every index and case study

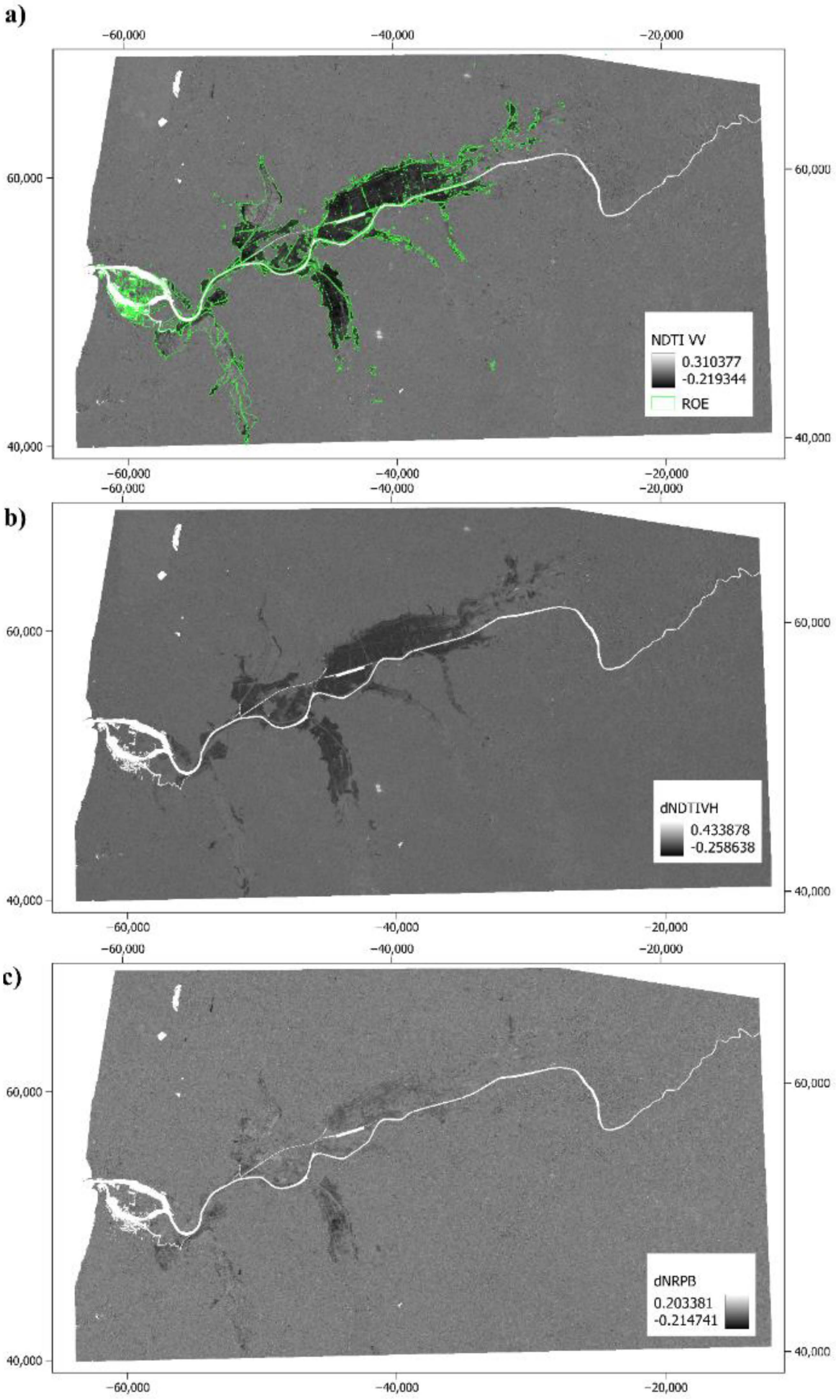

Figure 3. Comparison of SAR-derived index differences (NDTI—Normalized Differenced Temporal Index for both (**a**) vertical-vertical (VV) and (**b**) vertical-horizontal (VH) polarizations; (**c**) dNRPB—difference of Normalized Ratio Procedure between Bands) alongside the delineation of the Reference Observed Event (ROE) [40] for the Mondego flood (Portugal) (coordinate reference system: PT-TM06/ETRS89).

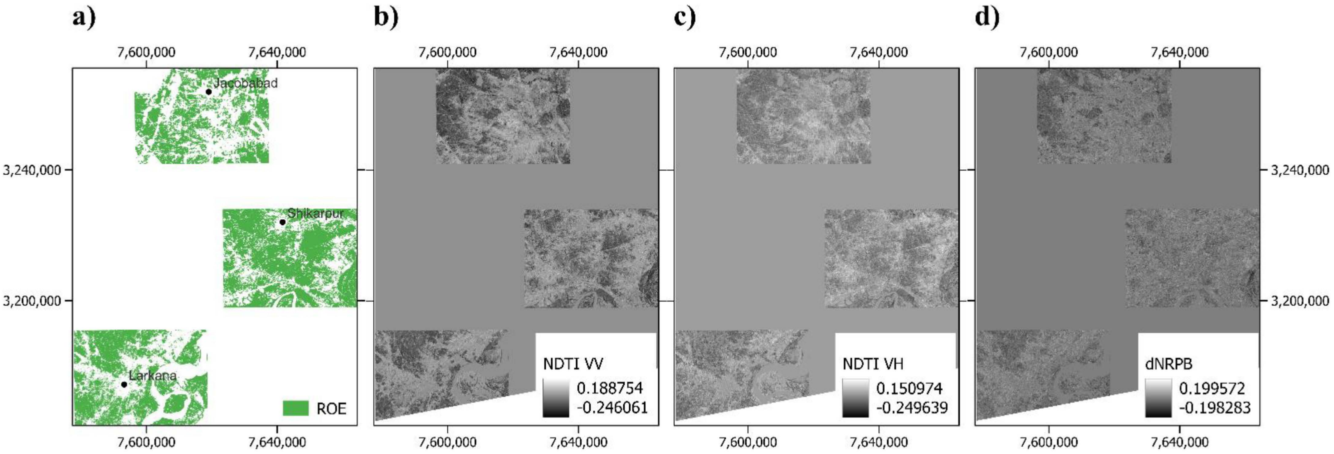

Figure 4. Comparison of SAR-derived index differences (NDTI—Normalized Differenced Temporal Index for both (**b**) vertical-vertical (VV) and (**c**) vertical-horizontal (VH) polarizations; (**d**) dNRPB—difference of Normalized Ratio Procedure between Bands) alongside (**a**) the delineation of the Reference Observed Event (ROE) [41] for the Sindh Province floods (Pakistan) (coordinate reference system: WGS84/World Mercator).

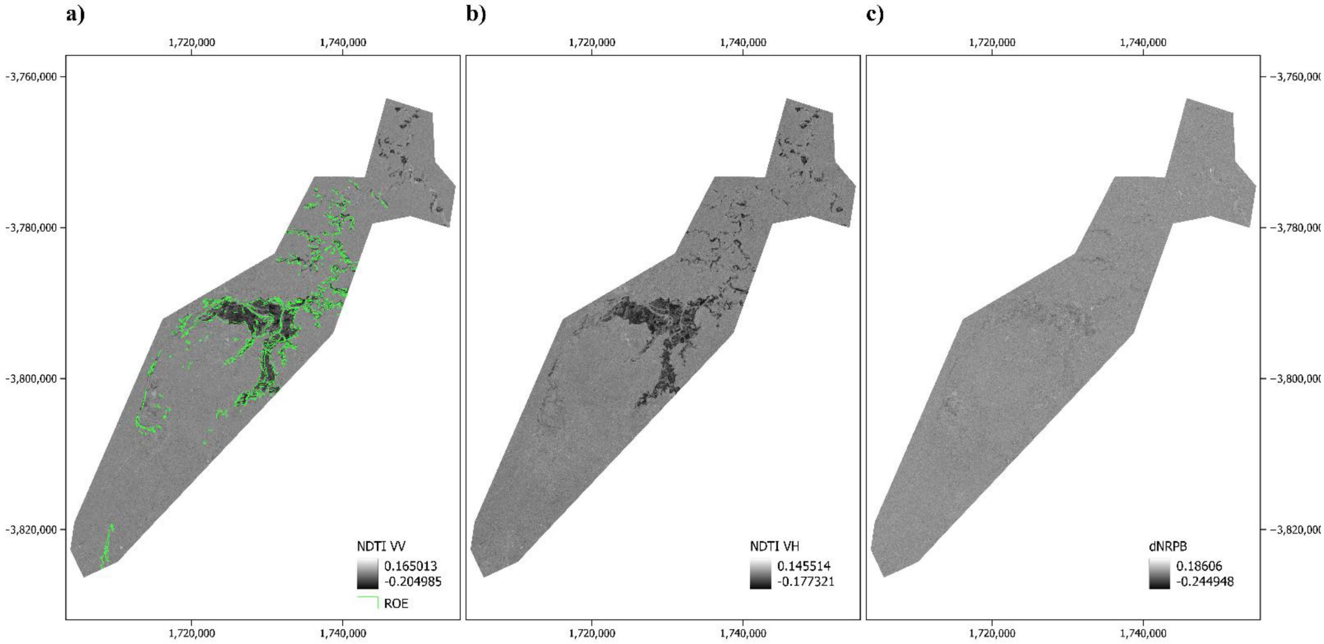

Figure 5. Comparison of SAR-derived index differences (NDTI—Normalized Differenced Temporal Index for both (**a**) vertical-vertical (VV) and (**b**) vertical-horizontal (VH) polarizations; (**c**) dNRPB—difference of Normalized Ratio Procedure between Bands) alongside the delineation of the Reference Observed Event (ROE) [42] for the Richmond floods (Australia) (coordinate reference system: WGS84/World Mercator).

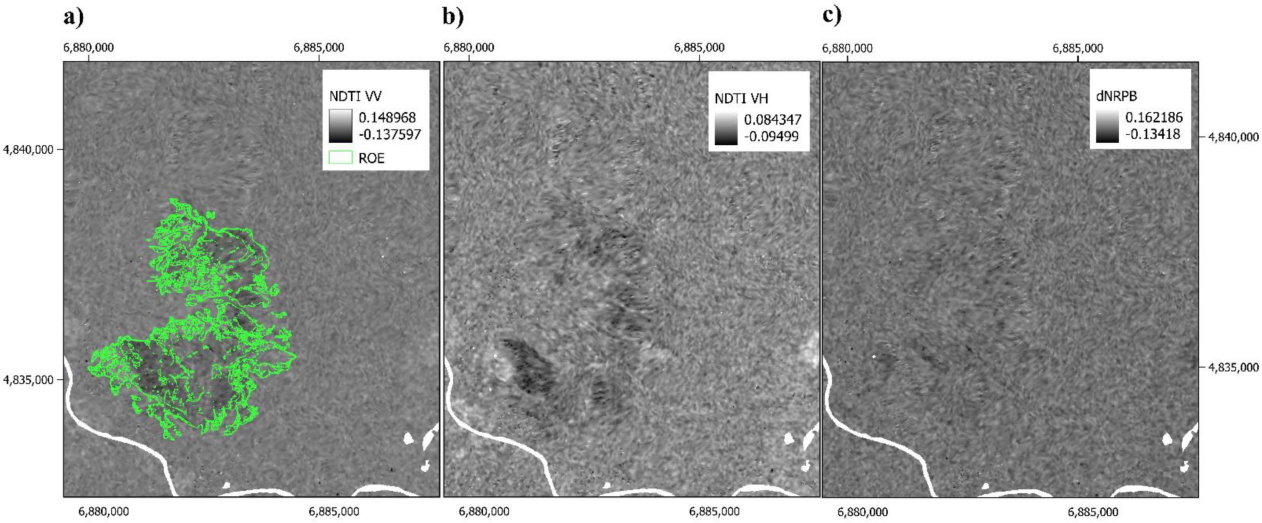

Figure 6. Comparison of SAR-derived index differences (NDTI—Normalized Differenced Temporal Index for both (**a**) vertical-vertical (VV) and (**b**) vertical-horizontal (VH) polarizations; (**c**) dNRPB—difference of Normalized Ratio Procedure between Bands) alongside the delineation of the Reference Observed Event (ROE) [45] for the Monte Pisano fire (Italy) (coordinate reference system: RDN2008/Italy zone (N-E)).

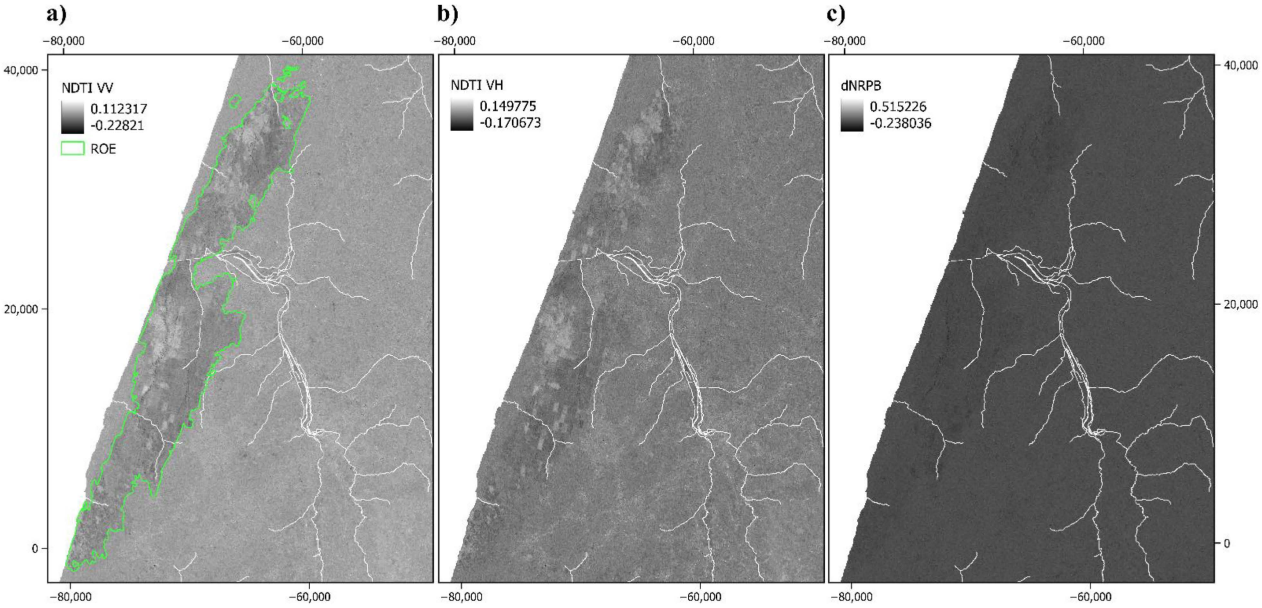

Figure 7. Comparison of SAR-derived index differences (NDTI—Normalized Differenced Temporal Index for both (**a**) vertical-vertical (VV) and (**b**) vertical-horizontal (VH) polarizations; (**c**) dNRPB—difference of Normalized Ratio Procedure between Bands) alongside the delineation of the Reference Observed Event (ROE) [48] for the Leiria National Forest fire (Portugal) (coordinate reference system: PT-TM06/ETRS89).

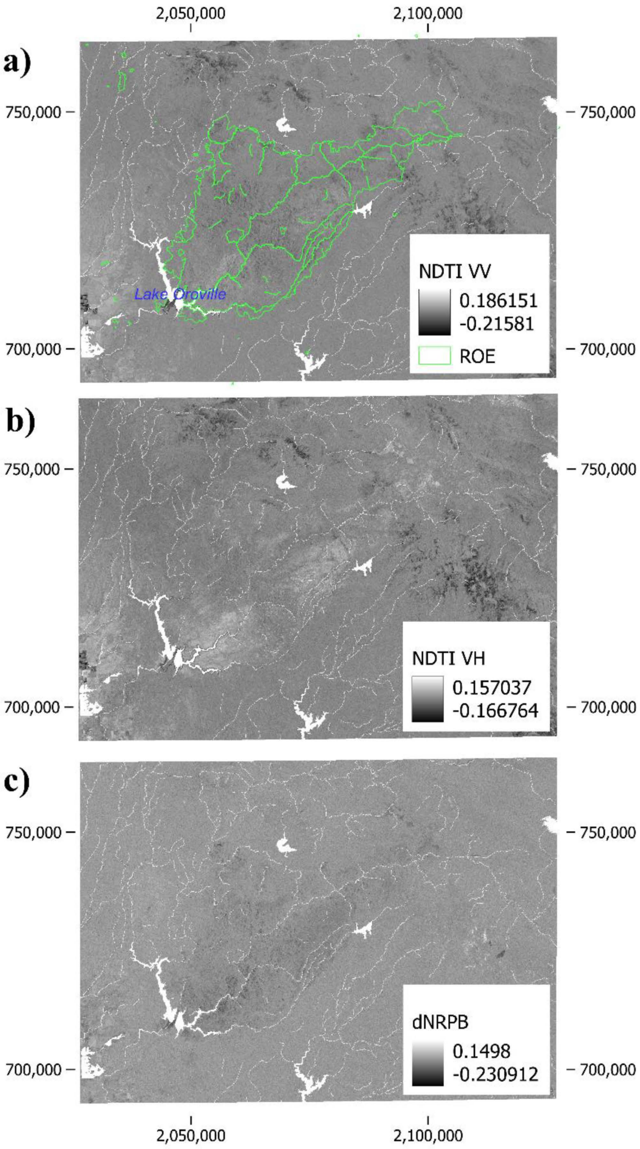

Figure 8. Comparison of SAR-derived index differences (NDTI—Normalized Differenced Temporal Index for both (**a**) vertical-vertical (VV) and (**b**) vertical-horizontal (VH) polarizations; (**c**) dNRPB—difference of Normalized Ratio Procedure between Bands) alongside the delineation of the Reference Observed Event (ROE) [51] for the North Complex fires (USA) (coordinate reference system: NAD83 / California zone 2).

Table 3. Optimal bin number values of both SAR and OMS indices for *d1f* and *d2f* in respect to the flood event case studies.

	SAR Indices						**OMS Indices**					
	NDTI VV		**NDTI HH**		**dNRPB**		**NDVI**		**NDWI**		**MNDWI**	
Flood Event	**d1f**	**d2f**	**d1f**	**d2f**	**d1f**	**d2f**	**d1f**	**d2f**	**d1f**	**d2f**	**d1f**	**d2f**
Mondego	446	316	446	316	158	158	28	28	39	39	28	28
Sindh	79	39	56	39	28	39	39	39	56	56	56	56
Richmond	39	56	56	39	19	19	-	-	-	-	-	-

Table 4. Optimal bin number values of both SAR and OMS indices for *d1f* and *d2f* in respect to the fire event case studies.

	SAR Indices						**OMS Indices**							
	NDTI VV		**NDTI HH**		**dNRPB**		**NDVI**		**NRBs**		**NRBl**		**NRB2**	
Fire Event	**d1f**	**d2f**	**d1f**	**d2f**	**d1f**	**d2f**	**d1f**	**d2f**	**d1f**	**d2f**	**d1f**	**d2f**	**d1f**	**d2f**
Monte Pisano	28	10	39	19	28	14	10	10	19	10	14	10	19	19
Leiria	56	28	28	28	28	28	19	39	39	39	79	79	79	79
California	39	56	28	28	39	39	79	112	39	28	56	56	56	79

Table 5. Index-differencing thresholds of both SAR and OMS indices, for flood-related changes.

	SAR Indices						**OMS Indices**					
	NDTI VV		**NDTI HH**		**dNRPB**		**NDVI**		**NDWI**		**MNDWI**	
Flood Event	**T1**	**T2**	**T1**	**T2**	**T1**	**T2**	**T1**	**T2**	**T1**	**T2**	**T1**	**T2**
Mondego	0.00	−0.07	0.00	−0.06	−0.14	-	−0.13	−0.69	0.07	1.46	0.10	0.62
Sindh	−0.01	−0.07	−0.01	−0.10	−0.01	−0.07	−0.01	−0.10	0.05	0.27	0.03	0.48
Richmond	−0.03	−0.07	−0.03	−0.07	−0.03	-	-	-	-	-	-	-

Table 6. Index-differencing thresholds of both SAR and OMS indices, for burned-related changes.

	SAR Indices						**OMS Indices**							
	NDTI VV		**NDTI HH**		**dNRPB**		**NDVI**		**NRBs**		**NRBl**		**NRB2**	
Fire Event	**T1**	**T2**	**T1**	**T2**	**T1**	**T2**	**T1**	**T2**	**T1**	**T2**	**T1**	**T2**	**T1**	**T2**
Monte Pisano	−0.04	−0.26	−0.03	−0.11	−0.04	−0.18	0.30	-	0.39	-	0.22	0.37	0.07	0.11
Leiria	−0.04	−0.21	−0.04	-	−0.04	-	0.08	0.19	0.04	0.09	−0.01	0.19	0.02	0.07
California	−0.01	-	−0.01	-	−0.04	-	0.05	0.48	0.21	0.36	0.11	0.64	0.05	0.35

4.3.3. Single- and Multi-Index Thematic Classifications

After selecting the thresholds, the MINDED-FBA tool performs automatic density slicing for each index, which allows coeval thematic change maps to be obtained for every index. The automatic procedures continue with the application of the majority analysis. Again, for the OMS module, the procedures are implemented according to [5,22]. For the SAR module, considering the improved performances of both NDTI polarizations in comparison to dNRPB (as described in Section 4.3.1), the majority analysis only accounted for NDTI VV and NDTI VH. Nevertheless, we decided to maintain the dNRPB single-index calculations within the tool in order to provide the user with the corresponding outputs. Whenever there was a tie condition between both NDTI indices, they were classified as "Mixed" (with the exception of the LMc + HMc condition, for which they were classified as LMc).

Moreover, whenever both OMS and SAR modules were selected, we also performed a pixel-by-pixel fusion of both datasets. This means that whenever only one of the modules could be determined, the fusion results only include the available module results. In the case of pixels containing results from both modules, we performed the majority analysis among all Multispectral and SAR indices. Hence, the results of the OMS module may include three or five coeval single-index classifications (depending on whether the analysis is performed for either flooded or burned areas), while the SAR module will only contribute two coeval single index classifications. Again, the "Mixed" class is used whenever there is no majority among the available single-index classifications.

Following this, the single- and multi-index thematic classifications were compared to the available dataset of ROE delineation for each case study, using the confusion matrix approach [56] and the Matthews Correlation Coefficient (MCC) [57,58]. The latter is regarded as a more reliable statistical method for unbalanced binary distributions, in which higher scores (i.e., worst MCC value = −1; best MCC value = +1) are only generated when the predictor is capable of correctly classifying both the majority of positive cases and the majority of negative cases [58]. “Mixed” pixel classifications have been excluded from these comparisons, just like null pixels (e.g., whenever the permanent water body mask is applied).

Table 7 summarizes the results for the Mondego floods event. For the SAR module, we can verify that, in comparison to the ROE dataset, both NDTI polarizations seem to have better overall performances in comparison to the dNRPB, particularly in terms of total change commission errors (Tc CE), observed event omission errors (OE OE), and MCC. These performances seem to be greatly improved by the SAR indices majority analysis. In comparison, the OMS majority analysis results (i.e., NDVI + NDWI + MNDWI) are slightly worse for most parameters. The spatial extent of the OMS data is also smaller, as consequence of the presence of clouds and cloud shadows in both pre- and post-event images. Finally, the fusion results (i.e., majority analysis among both OMS and SAR classifications), seem to achieve the best overall results, including the best OA and MCC. Among all the indices, we verify that most have a tendency to overestimate changes, as the area of the total changes (Tc) is predominantly higher than the delimitation area of the ROE (with the exception of dNRPB, which seems to be the worst performer among all indices).

Table 7. Summary of the confusion matrix parameters and Matthews Correlation Coefficient (MCC) obtained for the Mondego flood, in comparison to the Reference Observed Event (ROE) (Nc—no changes; LMc—low-magnitude changes; HMc—high-magnitude changes; Tc—total changes; OA—overall accuracy; Tc CE—total change commission errors; OE OE—observed event omission errors).

Dataset		**Accuracy (%)**					**Errors (%)**		**MCC**	**Total Areas (10^3 ha)**				
		Nc	**LMc**	**HMc**	**Tc**	**OA**	**Tc CE**	**OE OE**		**Nc**	**LMc**	**HMc**	**ROE**	**Tc**
SAR	NDTI VV	98.4	19.0	95.2	45.2	92.2	54.8	20.5	0.56	123.6	10.8	5.7	9.4	16.5
	NDTI VH	98.0	30.8	95.9	57.9	94.6	42.1	27.9	0.62	128.4	6.8	4.9	9.4	11.7
	dNRPB	93.3	23.0	-	23.0	93.3	77.0	99.9	0.01	140.1	0.0	-	9.4	0.0
	NDTI VV + NDTI VH	98.4	52.4	98.7	75.8	96.9	24.2	21.8	0.75	120.8	4.4	4.5	8.6	8.9
OMS	NDVI + NDWI + MNDWI	97.8	40.8	93.0	58.9	92.8	41.1	20.1	0.65	80.2	7.7	4.1	8.7	11.8
SAR + MS	Fusion	99.2	56.6	94.3	73.0	97.2	27.0	12.3	0.79	126.6	5.8	4.5	8.6	10.3

In Figure 9, we can observe the change maps generated by the MINDED-FBA tool for the Mondego flood event in comparison to the ROE delineation. When comparing the SAR and OMS maps, we can observe several areas near the Mondego River mouth which have been detected as changes (either LMc or HMc) by the OMS indices only. The upstream areas (to the extreme eastern side) could only be analyzed with the SAR module and were dominated by “Mixed” pixels (which correspond to Nc in ROE). In the fusion map, the classification around the river mouth seems to be similar to the OMS dataset (i.e., mostly as HMc), while the central part of the map includes a few more “Mixed” pixels than either the OMS or SAR modules. Finally, the extreme eastern side consists of the same results from the SAR module, which is the only module contributing to the fusion results.

Regarding the Sindh Province floods, in Table 8 we can verify that, for the SAR module, the NDTI VV achieved the best individual correlation with the ROE dataset. Nevertheless, the combination of both NDTI polarizations resulted in the best overall correlation with the delineation dataset (including the best OA and MCC). The combined results from the OMS indices show slightly worse correlations with the ROE. Finally, the fusion results have the second-best overall performance for most of the parameters in Table 8, yet also include the best performance for both HMc accuracy and OE OE.

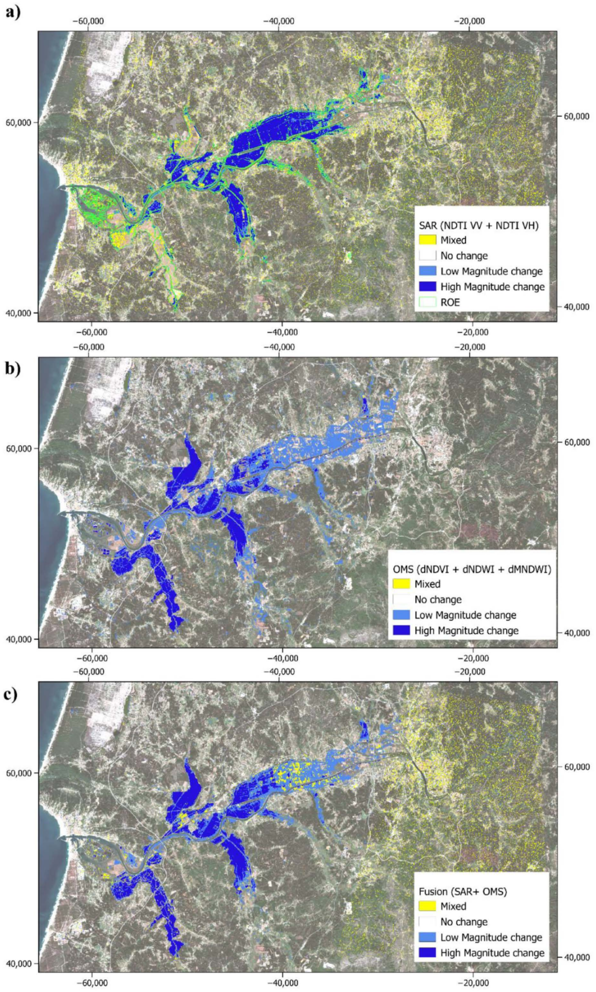

Figure 9. Flood-related change maps for the Mondego case study, obtained from the (**a**) OMS, (**b**) SAR, and (**c**) fusion datasets in comparison to the Reference Observed Event (ROE) [40] (coordinate reference system: PT-TM06/ETRS89).

Table 8. Summary of the confusion matrix parameters and Matthews Correlation Coefficient (MCC) obtained for the Sindh Province floods, in comparison to the Reference Observed Event (ROE) (Nc—no changes; LMc—low-magnitude changes; HMc—high-magnitude changes; Tc—total changes; OA—overall accuracy; Tc CE—total change commission errors; OE OE—observed event omission errors).

Dataset		**Accuracy (%)**					**Errors (%)**		**MCC**	**Total Areas (10^3 ha)**				
		Nc	**LMc**	**HMc**	**Tc**	**OA**	**Tc CE**	**OE OE**		**Nc**	**LMc**	**HMc**	**ROE**	**Tc**
SAR	NDTI VV	90.8	78.4	85.5	81.7	88.6	18.3	25.9	0.70	536.6	93.3	78.9	189.8	172.1
	NDTI VH	90.7	77.9	88.0	78.2	87.5	21.8	26.1	0.68	529.3	173.7	5.6	189.8	179.4
	dNRPB	86.4	67.8	76.4	68.3	82.1	31.7	38.5	0.53	538.1	159.7	10.9	189.8	170.6
	NDTI VV + NDTI VH	93.3	83.3	88.3	83.5	91.0	16.5	21.5	0.75	507.3	144.8	5.3	159.6	150.1
OMS	NDVI + NDWI + MNDWI	90.7	70.8	88.1	83.0	89.0	17.0	27.4	0.70	559.0	49.1	116.3	188.9	165.4
SAR + MS	Fusion	92.2	75.7	88.5	83.0	89.8	17.0	21.2	0.74	548.1	82.7	108.1	201.0	190.8

Figure 10 includes the Sindh Province floods ROE, alongside with the thematic change maps for each module of the MINDED-FBA tool, for the three areas of interest considered by the Copernicus EMS. Among the three MINDED-FBA tool maps, we can verify an overall tendency to underestimate changes in comparison to the ROE. This effect seems to be less evident for the SAR results, although this module displays more "Mixed" pixels than all the other maps. The underestimating of the OMS results seems to be more evident, particularly for the two northern areas (i.e., Jacobabad and Shikarpur). Nevertheless, regardless of the module, all seem to produce false detections of flood-related changes in the northwestern side of the Jacobabad area (i.e., the northern area of interest). In comparison to the remaining datasets, the fusion (SAR + MS) seems to resolve most "Mixed" conditions.

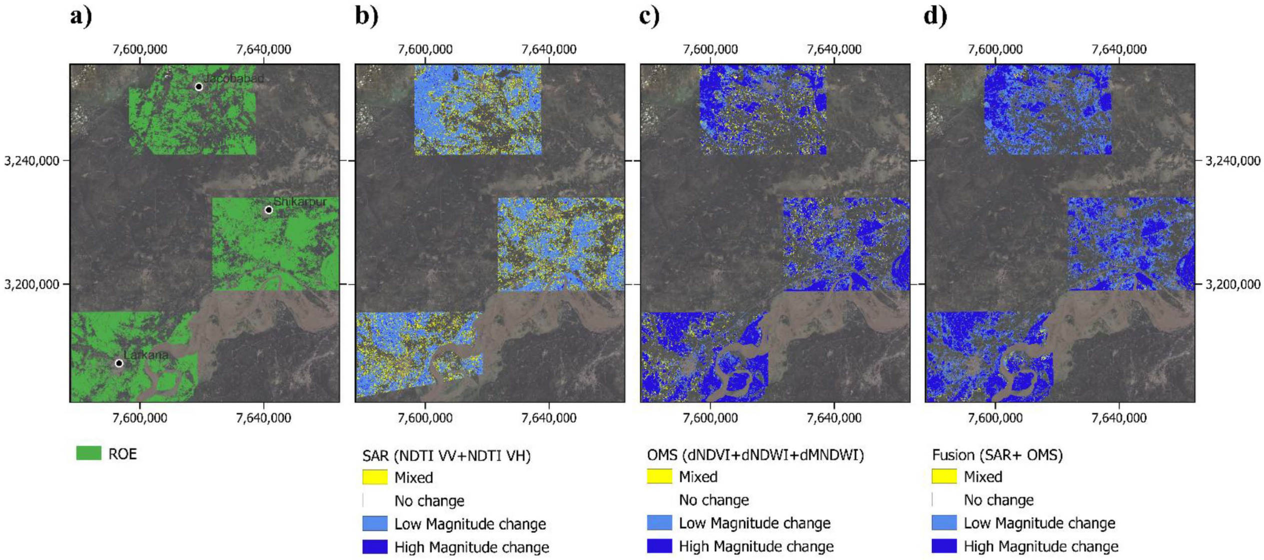

Figure 10. Flood-related change maps for the Sindh Province case study, obtained from the (**b**) OMS, (**c**) SAR, and (**d**) fusion datasets, in comparison to (**a**) the Reference Observed Event (ROE) [41] (coordinate reference system: WGS84/World Mercator).

Regarding the Richmond floods, for which we have selected the SAR module only, Table 9 summarizes the comparison of results with the ROE delineation. Similar to the previous case study, the dNRPB seems to be the worst performer, while the majority analysis with the combination of both NTDI polarizations seems to improve every parameter of the confusion matrix analysis and MCC.

Table 9. Summary of the confusion matrix parameters and Matthews Correlation Coefficient (MCC) obtained for the Richmond flood, in comparison to the Reference Observed Event (ROE) (Nc—No changes; LMc—low-magnitude changes; HMc—high-magnitude changes; Tc—total changes; OA—overall accuracy; Tc CE—total change commission errors; OE OE—observed event omission errors).

Dataset		Accuracy (%)					Errors (%)		MCC	Total Areas (10^3 ha)				
		Nc	LMc	HMc	Tc	OA	Tc CE	OE OE		Nc	LMc	HMc	ROE	Tc
SAR	NDTI VV	96.9	26.4	68.9	51.3	91.5	48.7	31.4	0.55	80.3	4.4	6.3	8.0	10.7
	NDTI VH	96.7	31.9	69.1	50.4	91.3	49.6	33.5	0.53	80.5	5.3	5.2	8.0	10.5
	dNRPB	92.5	24.6	-	24.6	87.6	75.4	79.8	0.16	84.4	6.6	-	8.0	6.6
	NDTI VV + NDTI VH	97.1	53.6	71.1	64.3	94.1	35.7	30.7	0.63	77.6	3.0	4.8	7.3	7.8

Figure 11 includes the combined NDTI map of the Richmond floods in comparison to the ROE, where we can verify a slight tendency to overestimate changes by the MINDED-FBA tool, particularly to the north side of the study area (mostly as HMc).

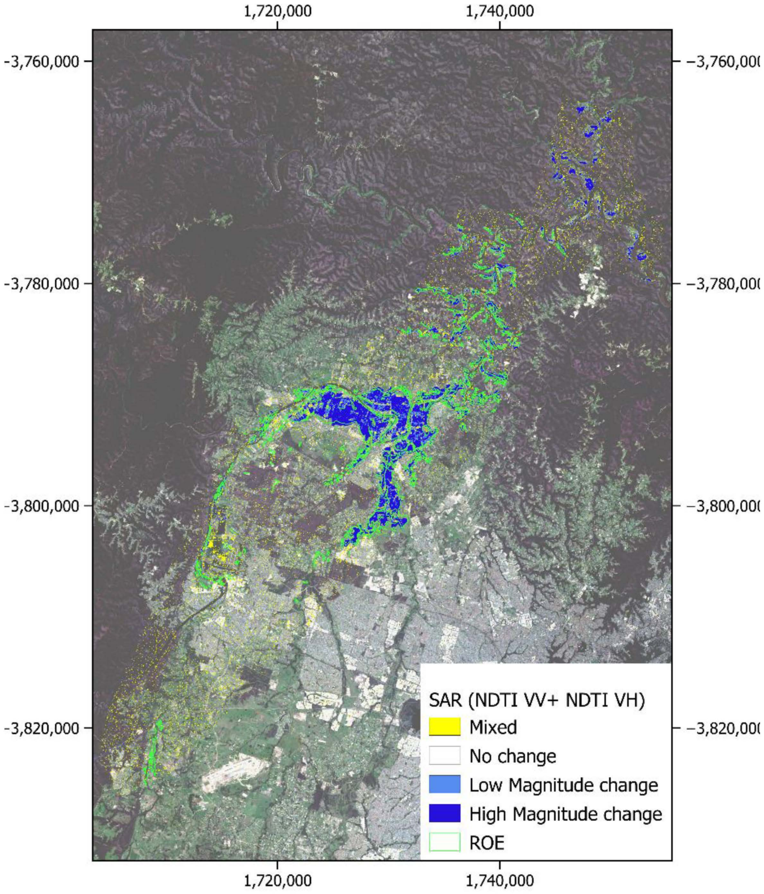

Figure 11. Flood-related change maps for the Richmond case study, obtained from the SAR module dataset, in comparison to the Reference Observed Event (ROE) [42] (coordinate reference system: WGS84/World Mercator).

Regarding the Monte Pisano fire, in Table 10 we can observe that the combination of the OMS indices seems to achieve the best performances in comparison to the ROE, being followed by the fusion dataset (which has the second-best statistics for most parameters). In the SAR module results, we verify high rates of omission errors for all indices, and lower commission errors, particularly for the combined NDTI classification.

Table 10. Summary of the confusion matrix parameters and Matthews Correlation Coefficient (MCC) obtained for the Monte Pisano fire, in comparison to the Reference Observed Event (ROE) (Nc—no changes; LMc—low-magnitude changes; HMc—high-magnitude changes; Tc—total changes; OA—overall accuracy; Tc CE—total change commission errors; OE OE—observed event omission errors).

Dataset		**Accuracy (%)**					**Errors (%)**		**MCC**	**Total Areas (10^3 ha)**				
		Nc	**LMc**	**HMc**	**Tc**	**OA**	**Tc CE**	**OE OE**		**Nc**	**LMc**	**HMc**	**ROE**	**Tc**
SAR	NDTI VV	88.4	83.9	0.0	83.8	88.3	16.2	92.1	0.24	8.4	0.1	0.0	1.1	0.1
	NDTI VH	88.5	63.4	0.0	63.3	88.1	36.7	90.2	0.22	8.4	0.2	0.0	1.1	0.2
	dNRPB	87.7	33.7	0.0	33.6	87.3	66.4	98.2	0.05	8.5	0.1	0.0	1.1	0.1
	NDTI VV + NDTI VH	89.1	93.8	-	93.8	89.1	6.2	96.6	0.17	8.3	0.0	-	0.9	0.0
OMS	NDVI + NDWI + MNDWI	99.5	60.0	98.5	85.3	97.5	14.7	3.7	0.89	7.2	0.4	0.8	1.0	1.2
SAR + MS	Fusion	98.9	57.8	98.5	85.6	97.2	14.4	7.7	0.87	7.4	0.4	0.8	1.0	1.1

Figure 12 includes the Monte Pisano change maps alongside the ROE delineation. Here, we can verify the underestimation of burned-related changes in the combined NDTI map when compared to the ROE. Instead, the OMS and fusion maps seem to achieve a much better correlation with the reference dataset.

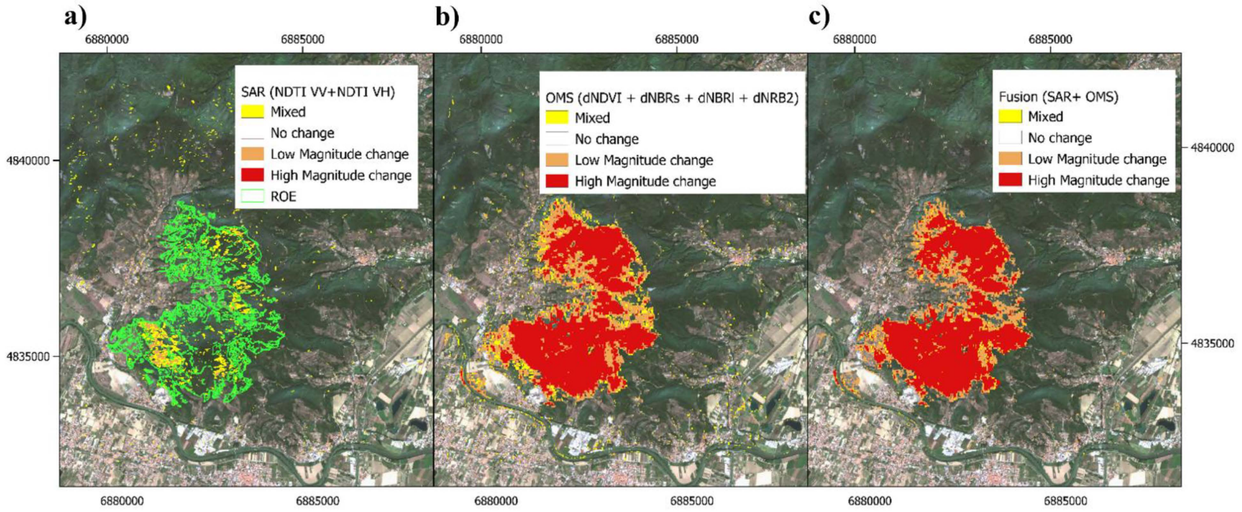

Figure 12. Burned-related change maps for the Monte Pisano case study obtained from (**a**) the OMS, (**b**) SAR, and (**c**) fusion datasets, in comparison to the Reference Observed Event (ROE) [45] (coordinate reference system: RDN2008/Italy zone (N-E)).

Regarding the Leiria National Forest fire, in Table 11 we can once more verify the improved performance of the combined OMS results in comparison to the SAR indices. Once more, the SAR indices have a tendency to underestimate burned-related changes which contribute to their overall worse performance in respect to the ROE. The fusion results have the second-best overall results, including OA and MCC.

Table 11. Summary of the confusion matrix parameters and Matthews Correlation Coefficient (MCC) obtained for the Leiria National Forest fire, in comparison to the Reference Observed Event (ROE) (Nc—no changes; LMc—low-magnitude changes; HMc—high-magnitude changes; Tc—total changes; OA—overall accuracy; Tc CE—total change commission errors; OE OE—observed event omission errors).

Dataset		**Accuracy (%)**					**Errors (%)**		**MCC**	**Total Areas (10^3 ha)**				
		Nc	**LMc**	**HMc**	**Tc**	**OA**	**Tc CE**	**OE OE**		**Nc**	**LMc**	**HMc**	**ROE**	**Tc**
SAR	NDTI VV	75.4	86.0	0.0	86.0	77.1	14.0	60.6	0.47	48.9	9.1	0.0	19.8	9.1
	NDTI VH	68.6	71.2	-	71.2	68.8	28.8	85.1	0.22	53.8	4.1	-	19.8	4.1
	dNRPB	67.2	71.1	-	71.1	67.3	28.9	92.6	0.15	55.9	2.1	-	19.8	2.1
	NDTI VV + NDTI VH	76.0	92.3	-	92.3	76.8	7.7	83.3	0.33	47.2	2.5	-	13.6	2.5
OMS	NDVI + NDWI + MNDWI	98.8	52.5	97.4	93.6	97.0	6.4	2.1	0.93	35.1	1.7	18.3	19.1	20.0
SAR + MS	Fusion	96.7	48.0	97.4	94.9	96.1	5.1	6.4	0.91	38.4	1.0	18.3	19.6	19.3

In Figure 13, we confirm the findings of Table 11 and verify the better correlation of the OMS and fusion maps with the ROE dataset. Furthermore, when compared to the Monte Pisano Fire findings, we have detected a higher proportion of HMc.

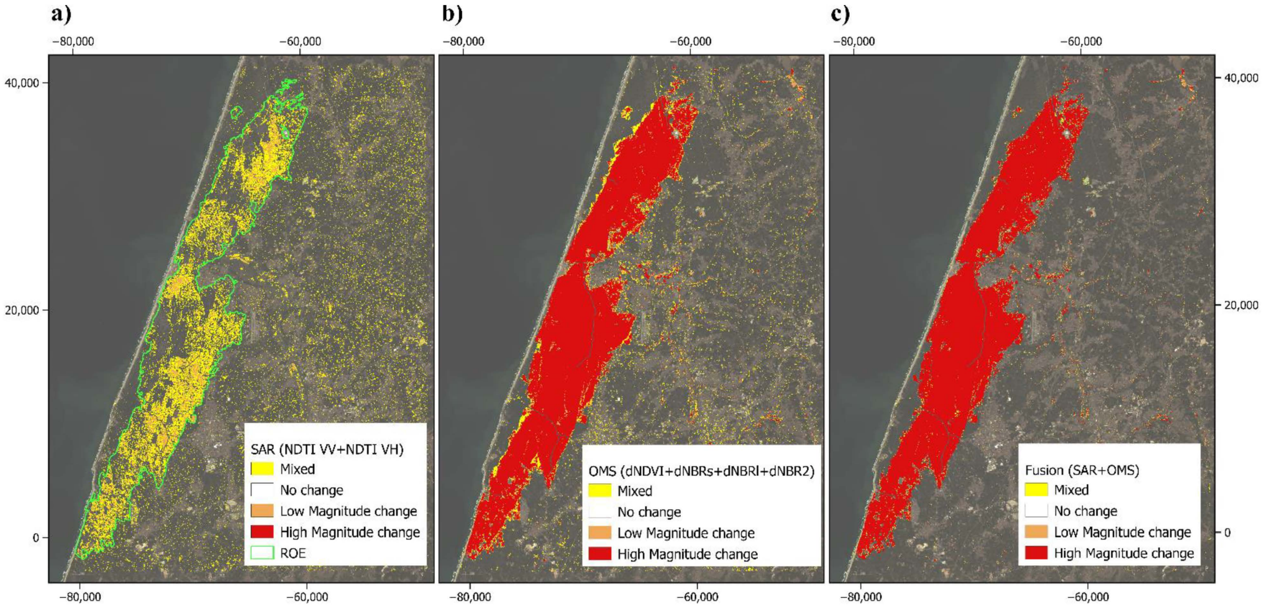

Figure 13. Burned-related change maps for the Leiria National Forest case study obtained from (**a**) the OMS, (**b**) SAR, and (**c**) fusion datasets, in comparison to the Reference Observed Event (ROE) [48] (coordinate reference system: PT-TM06/ETRS89).

Table 12 includes the summarization of the North Complex fire event. The combination of OMS indices resulted in the best correlation in respect to the ROE, followed by the fusion dataset. In comparison to the other fire event case studies, the Tc CEs are higher, suggesting the tendency to overestimate changes in comparison to the reference data. As for the SAR module results, we verify significantly worse correlations with the ROE (including negative MCC), this time with the NDTI polarizations displaying even worse performances than the dNRPB.

Table 12. Summary of the confusion matrix parameters and Matthews Correlation Coefficient (MCC) obtained for the North Complex fire, in comparison to the Reference Observed Event (ROE) (Nc—no changes; LMc—low-magnitude changes; HMc—high-magnitude changes; Tc—total changes; OA—overall accuracy; Tc CE—total change commission errors; OE OE—observed event omission errors).

Dataset		Accuracy (%)					Errors (%)		MCC	Total Areas (103 ha)				
		Nc	LMc	HMc	Tc	OA	Tc CE	OE OE		Nc	LMc	HMc	ROE	Tc
SAR	NDTI VV	83.0	26.9	6.3	26.9	77.0	73.1	84.1	0.08	627.4	74.9	0.0	126.5	74.9
	NDTI VH	81.3	11.4	-	11.4	74.9	88.6	94.2	−0.05	638.0	64.3	-	126.5	64.3
	dNRPB	83.0	54.8	-	54.8	82.2	45.2	91.7	0.16	683.2	19.2	-	126.5	19.2
	NDTI VV + NDTI VH	82.7	11.5	-	11.5	79.2	88.5	96.6	−0.03	594.1	31.0	-	106.2	31.0
OMS	NDVI + NDWI + MNDWI	94.8	82.9	98.9	83.1	92.9	16.9	24.5	0.75	450.8	85.8	1.2	95.8	87.0
SAR + MS	Fusion	92.8	71.0	99.0	71.3	89.6	28.7	36.0	0.61	569.2	100.6	1.2	113.4	101.8

In Figure 14, we can verify the low correlation of the SAR indices in comparison to the reference burned area dataset, with most of the detected changes being located in a range extending from northwest to southeast, away from the ROE data. As for the OMS and fusion maps, the correlation with the ROE is significantly improved, particularly for the North Complex fire area (which is located in the central part of the showcased area). However, the OMS maps also detect a few changes in the same regions resulting from the SAR.

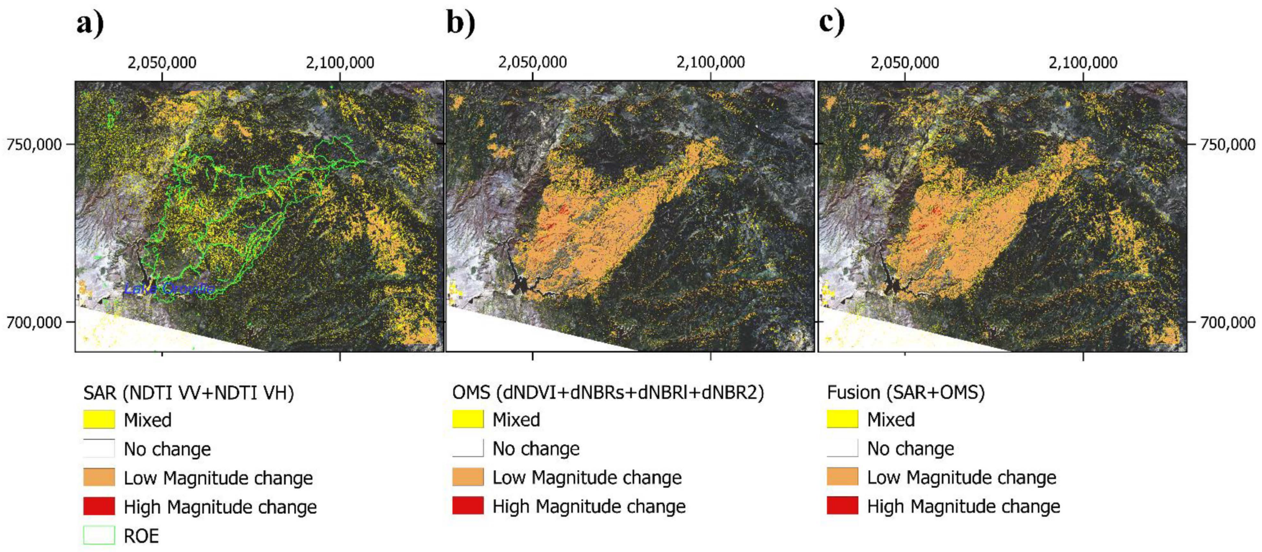

Figure 14. Burned-related change maps for the North Complex case study, obtained from (**a**) the OMS, (**b**) SAR and (**c**) fusion datasets, in comparison to the Reference Observed Event (ROE) [51] (coordinate reference system: NAD83/California zone 2).

Table 13 summarizes the fusion results for all the case studies. When comparing both types of events, we cannot observe relevant differences between flood and burned events. The Monte Pisano seems to have achieved the best overall statistics (in terms of errors and MCC), while the North Complex case study was generally the worst (except for the LMc and HMc class accuracies). Nevertheless, all events achieved high overall accuracies (i.e., above ca. 90%), and high MCC (over 0.6), indicating good correlations with their respective ROE datasets.

Table 13. Summary of the fusion data results (if available) for each case study (Nc—no changes; LMc—low-magnitude changes; HMc—high-magnitude changes; Tc—total changes; OA—overall accuracy; Tc CE—total change commission errors; OE OE—observed event omission errors). study area feature processing extent (SAFPE).

Event	Type	Dataset	Accuracy (%)					Errors (%)		MCC	SAFPE (ha)
			Nc	LMc	HMc	Tc	OA	Tc CE	OE OE		
Mondego	Flood	SAR + MS	99.2	56.6	94.3	73.0	97.2	27.0	12.3	0.79	147.608
Sindh Province	Flood	SAR + MS	92.2	75.7	88.5	83.0	89.8	17.0	21.2	0.74	289.057
Richmond	Flood	SAR	97.1	53.6	71.1	64.3	94.1	35.7	30.7	0.63	91.894
Monte Pisano	Fire	SAR + MS	96.7	48.0	97.4	94.9	96.1	5.1	6.4	0.91	8.673
Leiria N. Forest	Fire	SAR + MS	98.9	57.8	98.5	85.6	97.2	14.4	7.7	0.87	173.145
North Complex	Fire	SAR + MS	92.8	71.0	99.0	71.3	89.6	28.7	36.0	0.61	711.794

4.3.4. Uncertainty Analysis

Figure 15 represents the uncertainty maps for the fusion datasets for every case study of this paper (apart the Figure 15c, related to the Richmond flood, which was determined with the SAR module only). These maps show that the higher values of uncertainty (i.e., 2 and 3) tend to occur around and inside the regions of change. In those locations where only the SAR module is available (i.e., Figure 15c and parts of Figure 15a) the scale consists of only two values, i.e., 0 where both NDTI polarizations have identical coeval classifications, and 3 for no majority conditions (different coeval classifications).

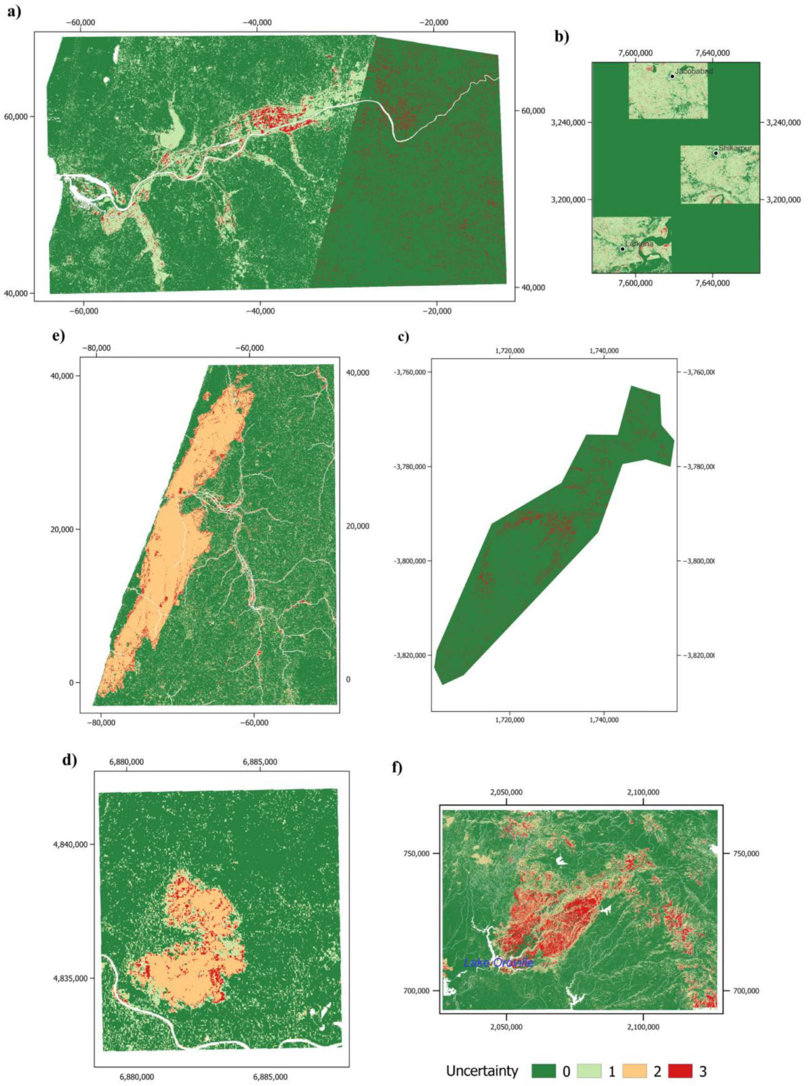

Figure 15. Uncertainty maps for (**a**) the Mondego Flood; (**b**) the Sindh Province floods; (**c**) the Richmond Flood; (**d**) the Monte Pisano Fire; (**e**) the Leiria National Forest fire; (**f**) the North Complex fire; with (**a**,**b**,**d**–**f**) being obtained from the fusion dataset and (**c**) being obtained from the SAR dataset.

5. Discussion

This paper presents the MINDED-FBA tool and demonstrates it as an efficient and effective instrument aimed at extracting both flooded and burned areas by means of both unsupervised classification of RS data and further automatic processing. The tool has been integrated in a freely distributed QGIS plugin, which facilitates running the entire methodological workflow (Figures 1 and 1A in Appendix A). Hence, it facilitates the application of digital change detection procedures even by users with less experience in respect to the tool's methodological principles, or, more generally, by non-experts in GIS or in RS techniques. The paper highlights the main methodological principles, which are based on the work by [9,27], and introduces some significant innovations, such as the incorporation of change detection based on SAR data. Such developments represent a great advancement in comparison to the original work, since they broaden the usable input satellite imagery. Namely, the use of SAR data opens the possibility of studying events even in cases of persistent cloud/smoke coverage, which are particularly relevant when studying flooding and wildfire phenomena.

Despite including a SAR module, the MINDED-FBA tool does not yet incorporate full preprocessing of Sentinel-1 images, which is strongly recommended. Such procedures have been performed with the ESA's SNAP tool which, despite being also freely available, requires an additional step prior to the MINDED-FBA tool process chain. Nevertheless, the MINDED-FBA tool allows the incorporation of layers for masking permanent water bodies, which would likely result in the detection of false positives by both the SAR and OMS modules.

For the OMS module, the MINDED-FBA tool inherits the same preprocessing procedures presented by [27], including the "Cloud + cloud shadow masking", "Topographic correction and topographic shadow masking", and "Highly Reflectance Surface (HRS) masking". We verified that the "Topographic correction and topographic shadow masking", which is particularly relevant for more mountainous areas [27], required the longest processing times among all the preprocessing options integrated within the MINDED-FBA. The HRS masking procedure is mostly relevant for the accurate detection of burned areas. It consists of applying different levels of masking, which have been derived from the work of [59], which are then implemented through tasseled cap brightness calculations applied to specific multispectral bands. The reference values used for the HRS masking were previously determined for a study area in Portugal [59]. The implementation of the MINDED-FBA within further wildfire study areas allowed us to verify that the HRS masking is effective without compromising the detection of burned areas.

Regarding the accuracy of results from the SAR module, we verified that in comparison to the OMS indices, the SAR-derived indices achieved comparable, if not better, overall results, particularly for the flood-related case studies. We found that the theoretical principles behind the MINDED and MINDED-BA methods could be directly applied to analyzing SAR-derived indices. One noticeable result concerns the optimal bin number, which assumes similar values for both the modules, with the only exception being the Mondego flood case study, which shows higher values for the SAR indices. Such response is likely a consequence of the multitemporal image difference being characterized by a strong signal and/or being affected by low statistical noise, hence producing maximum bin ratio values for higher bin number values (see Equation (12) in [27]).

Considering the disaggregation of the Sentinel-1 as polarized data, the availability of indices for the SAR module is reduced when compared to the full array of indices which may be determined from OMS bands. Furthermore, besides the results shown in Section 4, we tested the implementation of the SAR module with Sentinel-1 scenes acquired in descending mode for the Monte Pisano and North Complex fires. In those cases, we verified significantly reduced sensitivity for detecting each corresponding burned area in respect to the ascending mode, which should be related with the steep morphology and the predominantly south-facing slopes of the burned areas.

The overall performance of the SAR module, and particularly for both NDTI polarizations, seems to be slightly reduced for the wildfire case studies, resulting in worse correlations when compared to the OMS module. This effect may be related to the lower sensitivity of this index to detect burned-related changes. Indeed, for certain burned-related conditions, the NDTI polarizations may also provide inverted index differencing signals (i.e., positive values instead of negatives). This effect is noticeable in the Leiria National Forest case study, particularly in a scarcely vegetated location which underwent previous burning (14 years before) [60]. As for the North Complex case study, we also verify the occurrence of presumably burned pixels with inverted signals (e.g., northeast of the Lake Oroville). In this case, the positive SAR index-differencing values also occur in areas which either underwent a previous fire (in 2008; [51]) or appeared to be clearcutting patches (by image visual interpretation) older than the North Complex fire.

In summary, the results from the considered case studies suggest that the OMS and SAR modules could have different relevancies depending on the type of change. While the OMS module seems to achieve the best performances for determining burned areas, the SAR module seems to be particularly suited to studying flood events. Moreover, the SAR module also enhances the possibilities of selecting recent usable post-event images, an option which is particularly relevant for studying flood events. Indeed, in such cases the spatial and temporal effects caused by water are more dynamic when compared to the short-term effects of fire. Furthermore, floods are often associated with heavy precipitation events, which may correspond to persistent cloud coverage periods, while SAR images may represent the only usable remote sensing data. This was the case of the Richmond floods, for which no cloud-free OMS images were available even several months after the event.

When analyzing floods, the thematic fusion dataset is obtained from a majority analysis with three OMS indices and two SAR indices, while for fires it is based on four OMS indices and two SAR indices. In practice, this means that in the current implementation of the MINDED-FBA, the SAR module has a lower weight in comparison to the OMS module, especially for the case of fires. Nevertheless, the analysis of the five case studies which included the fusion of OMS and SAR modules demonstrates that such combination provided consistently good performances in comparison to the respective ROE delineations. In particular, the fusion dataset provides the second-best OA accuracy and MCC in four of the case studies, as well as the best statistics in the case of the Mondego floods. Moreover, we underline that the tool is open-source, allowing further developments, such as incorporating new indices for either of the modules.

When analyzing the summarized results of Table 13, we can verify that the best overall accuracies were obtained for the Mondego and Leiria National Forest case studies, while the best MCC was obtained for the Monte Pisano fire. This implies that, for such parameters, there seems to be a correlation with the study area feature processing extent (SAFPE), as the best performances were obtained for the smaller case study areas under analysis, while the worst results seem to correspond to the two largest areas (i.e., the North Complex fire and the Sindh Province floods). These results are to be expected, because for larger areas, the quality of the thresholds extracted from the image differencing statistics could be affected by larger extents of false positives/negatives related to other kinds of changes than either flooding or fire.

The uncertainty results are another important benefit obtained from the majority analysis. It allows us to identify the pixels that result in higher or lower agreement among the considered indices, which we interpret as an indicator of the uncertainty level of classification. As verified in Figure 15, the higher uncertainty values were found both within and around the larger areas of change. Such an effect is to be expected, and should correspond to different land cover/conditions, both for floods and fires. In the case of floods, certain flooding water conditions (e.g., shallower, turbid, or eutrophicated water), as well as heavily water-saturated soils, or superficially wet natural or artificial surfaces, may be detected as flood-related changes by only a few indices. In the same way, lightly burned areas (e.g., within scarcely vegetated areas or partial burning), post-fire vegetation regrowth, or even certain non-burning conditions (e.g., drought or clearcutting), may also be detected as burned-related changes by only a few indices. We consider that such an approach of uncertainty estimation provides a more reliable representation of both flooding and fire changes, beyond the typical binary maps based on either visual delineation or single-index classifications from either OMS or SAR images.

6. Conclusions

This paper presents the new MINDED-FBA tool, a freely available QGIS plugin for determining flooded and burned areas from satellite remote sensing data. The tool starts by applying an index differencing approach to either optical multispectral and/or SAR imagery. Then, it performs multiple unsupervised classifications based on several automatic statistical procedures. Finally, it implements a majority analysis which allows the user to obtain multi-index thematic change maps, as well as an estimate of their uncertainty.

The MINDED-FBA tool has been applied to six case studies with diverse conditions, geographical locations, extent, and morphology. The outputs have been compared to reference flooded or burned area delineation datasets, mostly obtained from the Copernicus EMS. The results demonstrate the capability of the tool for achieving consistent correlations with such reference products. For this reason, we propose that the MINDED-FBA tool could be used as an unsupervised classification-based near-real-time solution for extracting flooding and burned areas, which could offer essential data to provide better informed emergency response measures.

Despite including here several case studies which encompass a large array of conditions, there is still room for further tests and developments. Hence, future research could include further geographical regions, as well as analyses of different kinds of changes, and the incorporation of further preprocessing steps (particularly for the SAR module) and remote sensing sensors.

Author Contributions: Conceptualization, E.R.O. and L.D.; Data curation, E.R.O.; Formal analysis, E.R.O. and L.D.; Funding acquisition, L.D. and F.L.A.; Investigation, E.R.O. and L.D.; Methodology, E.R.O. and L.D.; Resources, L.D. and F.L.A.; Software, E.R.O.; Supervision, L.D. and F.L.A.; Validation E.R.O. and L.D.; Visualization, E.R.O. and L.D.; Writing—original draft, E.R.O. and L.D.; Writing—review and editing, E.R.O. and L.D. All authors have read and agreed to the published version of the manuscript.

Funding: Thanks are due to the Agreement between DSFTA-UNISI and IGG-CNR (2018/9150000123), and to FCT/MCTES for the financial support to CESAM (UIDP/50017/2020+UIDB/50017/2020).

Data Availability Statement: Not applicable.

Conflicts of Interest: The authors declare no conflict of interest. The funders had no role in the design of the study; in the collection, analyses, or interpretation of data; in the writing of the manuscript; or in the decision to publish the results.

Appendix A

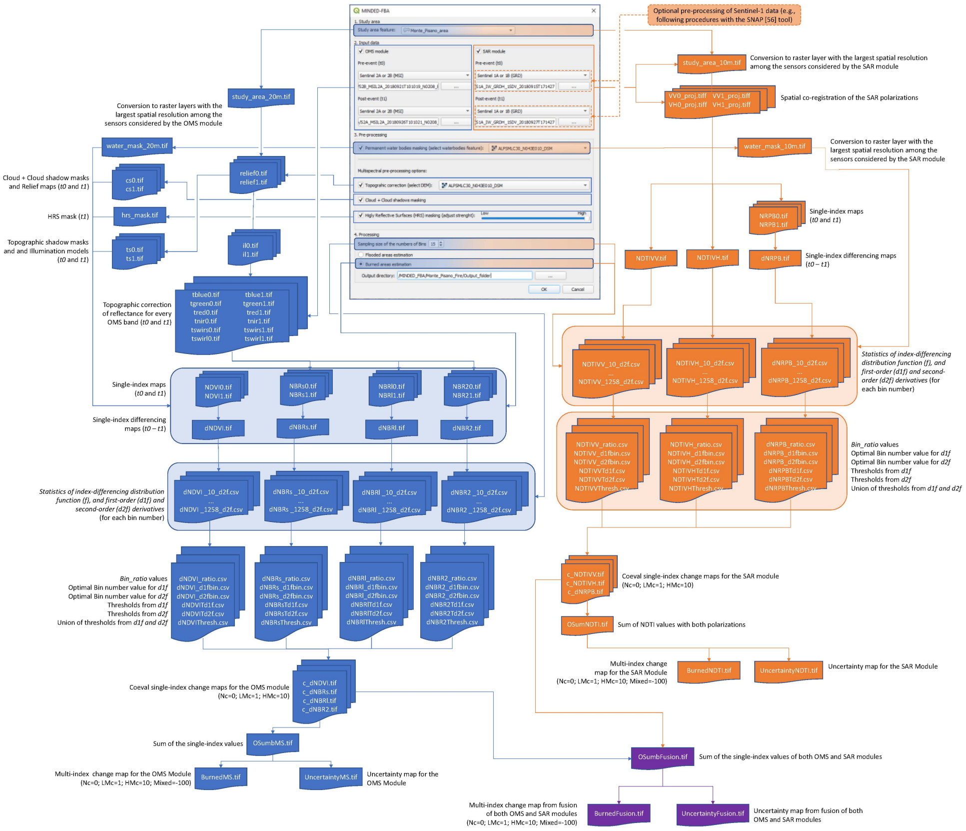

Figure A1. Workflow of the MINDED-FBA procedures and outputs. Blue and orange describe procedures and outputs related to the OMS and SAR modules respectively; violet describes data fusion procedures and outputs.

References

1. Van Westen, C.J. Remote Sensing and GIS for Natural Hazards Assessment and Disaster Risk Management. In *Treatise on Geomorphology*; Schroder, J.F., Bishop, M.P., Eds.; Elsevier Inc.: San Diego, CA, USA, 2013; Volume 3, pp. 259–298. ISBN 978-0-08-088522-3.
2. Joyce, K.E.; Belliss, S.E.; Samsonov, S.V.; McNeill, S.J.; Glassey, P.J. A Review of the Status of Satellite Remote Sensing and Image Processing Techniques for Mapping Natural Hazards and Disasters. *Prog. Phys. Geogr.* **2009**, *33*, 183–207. [CrossRef]
3. Harb, M.; Acqua, F.D. Remote Sensing in Multirisk Assessment. *IEEE Geosci. Remote Sens. Mag.* **2017**, *5*, 53–65. [CrossRef]
4. Martinis, S.; Kersten, J.; Twele, A. A Fully Automated TerraSAR-X Based Flood Service. *ISPRS J. Photogramm. Remote Sens.* **2015**, *104*, 203–212. [CrossRef]
5. Fornacca, D.; Ren, G.; Xiao, W. Evaluating the Best Spectral Indices for the Detection of Burn Scars at Several Post-Fire Dates in a Mountainous Region of Northwest Yunnan, China. *Remote Sens.* **2018**, *10*, 1196. [CrossRef]
6. Keeley, J.E. Fire Intensity, Fire Severity and Burn Severity: A Brief Review and Suggested Usage. *Int. J. Wildland Fire* **2009**, *18*, 116–126. [CrossRef]
7. Chuvieco, E.; Aguado, I.; Salas, J.; García, M.; Yebra, M.; Oliva, P. Satellite Remote Sensing Contributions to Wildland Fire Science and Management. *Curr. For. Rep.* **2020**, *6*, 81–96. [CrossRef]
8. Sivanpillai, R.; Jacobs, K.M.; Mattilio, C.M.; Piskorski, E.V. Rapid Flood Inundation Mapping by Differencing Water Indices from Pre- and Post-Flood Landsat Images. *Front. Earth Sci.* **2021**, *15*, 1–11. [CrossRef]
9. Oliveira, E.R.; Disperati, L.; Cenci, L.; Pereira, L.G.; Alves, F.L. Multi-Index Image Differencing Method (MINDED) for Flood Extent Estimations. *Remote Sens.* **2019**, *11*, 1305. [CrossRef]
10. Mohite, J.D.; Sawant, S.A.; Pandit, A.; Pappula, S. Investigating the Performance of Random Forest and Support Vector Regression for Estimation of Cloud-Free NDVI Using Sentinel-1 Sar Data. *Int. Arch. Photogramm. Remote Sens. Spat. Inf. Sci.* **2020**, *43*, 1379–1383. [CrossRef]
11. Zhao, Q.; Pan, J.; Devlin, A.T.; Tang, M.; Yao, C.; Zamparelli, V.; Falabella, F.; Pepe, A. On the Exploitation of Remote Sensing Technologies for the Monitoring of Coastal and River Delta Regions. *Remote Sens.* **2022**, *14*, 2384. [CrossRef]
12. de Luca, G.; Silva, J.M.N.; Modica, G. A Workflow Based on Sentinel-1 SAR Data and Open-Source Algorithms for Unsupervised Burned Area Detection in Mediterranean Ecosystems. *GIsci Remote Sens.* **2021**, *58*, 516–541. [CrossRef]
13. Vreugdenhil, M.; Navacchi, C.; Bauer-Marschallinger, B.; Hahn, S.; Steele-Dunne, S.; Pfeil, I.; Dorigo, W.; Wagner, W. Sentinel-1 Cross Ratio and Vegetation Optical Depth: A Comparison over Europe. *Remote Sens.* **2020**, *12*, 3404. [CrossRef]
14. Alvarez-Mozos, J.; Villanueva, J.; Arias, M.; Gonzalez-Audicana, M. Correlation Between NDVI and Sentinel-1 Derived Features for Maize. In *2021 IEEE International Geoscience and Remote Sensing Symposium IGARSS*; Institute of Electrical and Electronics Engineers Inc.: New York, NY, USA, 2021; pp. 6773–6776.
15. Bioresita, F.; Puissant, A.; Stumpf, A.; Malet, J.P. Fusion of Sentinel-1 and Sentinel-2 Image Time Series for Permanent and Temporary Surface Water Mapping. *Int. J. Remote Sens.* **2019**, *40*, 9026–9049. [CrossRef]
16. Volpi, M.; Petropoulos, G.P.; Kanevski, M. Flooding Extent Cartography with Landsat TM Imagery and Regularized Kernel Fisher's Discriminant Analysis. *Comput. Geosci.* **2013**, *57*, 24–31. [CrossRef]
17. Singh, A. Review Article: Digital Change Detection Techniques Using Remotely-Sensed Data. *Int. J. Remote Sens.* **1989**, *10*, 989–1003. [CrossRef]
18. Coppin, P.; Jonckheere, I.; Nackaerts, K.; Muys, B.; Lambin, E. Digital Change Detection Methods in Ecosystem Monitoring: A Review. *Int. J. Remote Sens.* **2004**, *25*, 1565–1596. [CrossRef]
19. Chini, M.; Hostache, R.; Giustarini, L.; Matgen, P. A Hierarchical Split-Based Approach for Parametric Thresholding of SAR Images: Flood Inundation as a Test Case. *IEEE Trans. Geosci. Remote Sens.* **2017**, *55*, 6975–6988. [CrossRef]
20. Boschetti, L.; Roy, D.P.; Justice, C.O.; Humber, M.L. MODIS-Landsat Fusion for Large Area 30m Burned Area Mapping. *Remote Sens. Environ.* **2015**, *161*, 27–42. [CrossRef]
21. Lillesand, T.M.; Kiefer, R.W.; Chipman, J.W. *Remote Sensing and Image Interpretation*, 7th ed.; John Wiley and Sons: New York, NY, USA, 2015; ISBN 978-1-118-34328-9.
22. Martinis, S.; Kuenzer, C.; Wendleder, A.; Huth, J.; Twele, A.; Roth, A.; Dech, S. Comparing Four Operational SAR-Based Water and Flood Detection Approaches. *Int. J. Remote Sens.* **2015**, *36*, 3519–3543. [CrossRef]
23. EMS Copernicus Emergency Management Service. Available online: https://emergency.copernicus.eu/ (accessed on 20 December 2022).
24. Narra, P.; Coelho, C.; Sancho, F.; Palalane, J. CERA: An Open-Source Tool for Coastal Erosion Risk Assessment. *Ocean Coast Manag.* **2017**, *142*, 1–14. [CrossRef]
25. Sala, J.; Lopez, A.; Romero, L.; Koudogbo, F. A Sentinel-1 Flood Map Generation QGIS Plugin. In Proceedings of the EGU General Assembly, Vienna, Austria, 17–22 April 2016; p. 14693.
26. Padrão, A.; Duarte, L.; Teodoro, A.C. A GIS Plugin for Susceptibility Modeling: Case Study of Wildfires in Vila Nova de Foz Côa. *Land* **2022**, *11*, 1093. [CrossRef]
27. Oliveira, E.R.; Disperati, L.; Alves, F.L. A New Method (MINDED-BA) for Automatic Detection of Burned Areas Using Remote Sensing. *Remote Sens.* **2021**, *13*, 5164. [CrossRef]
28. USGS. *Landsat 7 (L7) Data Users Handbook. USGS Landsat User Services*; USGS: Washington, DC, USA, 2019; Volume 7, p. 151.
29. USGS. *Landsat 9 Data Users Handbook Landsat 9 Data Users Handbook Version 1.0.*; USGS: Washington, DC, USA, 2022; Volume 107.

30. USGS. *Landsat 8 Data Users Handbook. EROS*; USGS: Washington, DC, USA, 2019; Volume 8, p. 106.
31. ESA. *Sentinel-2 User Handbook*; ESA: Paris, France, 2015; Volume 2.
32. ESA. User Guides–Sentinel-1 SAR–Sentinel Online. Available online: https://sentinels.copernicus.eu/web/sentinel/user-guides/sentinel-1-sar (accessed on 28 July 2022).
33. Filipponi, F. *Sentinel-1 GRD Preprocessing Workflow*; MDPI: Basel, Switzerland, 2019; p. 11.
34. Belenguer-Plomer, M.A.; Chuvieco, E.; Profile, S.; Tanase, M.A. Sentinel-1 Based Algorithm to Detect Burned Areas PREDFIRE: Climate Monitoring and PREDictions to Forecast Global FIRE Activity View Project Fire CCI View Project. In Proceedings of the 11th EARSeL Forest Fires SIG, Chania, Greece, 25–27 September 2017.
35. Belenguer-Plomer, M.A.; Tanase, M.A.; Fernandez-Carrillo, A.; Chuvieco, E. Burned Area Detection and Mapping Using Sentinel-1 Backscatter Coefficient and Thermal Anomalies. *Remote Sens. Environ.* **2019**, *233*, 111345. [CrossRef]
36. Ghamisi, P.; Rasti, B.; Yokoya, N.; Wang, Q.; Hofle, B.; Bruzzone, L.; Bovolo, F.; Chi, M.; Anders, K.; Gloaguen, R.; et al. *Multisource and Multitemporal Data Fusion in Remote Sensing*; IEEE: New York, NY, USA, 2018.
37. Schowengerdt, R.A. *Remote Sensing: Models and Methods for Image Processing*, 3rd ed.; Academic Press: Burlington, VT, USA, 2007; ISBN 9780123694072.
38. Riaño, D.; Chuvieco, E.; Salas, J.; Aguado, I. Assessment of Different Topographic Corrections in Landsat-TM Data for Mapping Vegetation Types (2003). *IEEE Trans. Geosci. Remote Sens.* **2003**, *41*, 1056–1061. [CrossRef]
39. Stojanovic, M.; Gonçalves, A.; Sorí, R.; Vázquez, M.; Ramos, A.M.; Nieto, R.; Gimeno, L.; Liberato, M.L.R. Consecutive Extratropical Cyclones Daniel, Elsa and Fabien, and Their Impact on the Hydrological Cycle of Mainland Portugal. *Water* **2021**, *13*, 1476. [CrossRef]
40. *Copernicus EMS EMSR417: Flood in Portugal*; European Commission: Brussels, Belgium, 2019.
41. *EMS EMSR629: Floods in Pakistan*; European Commission: Brussels, Belgium, 2022.
42. *EMS EMSR567: Floods in Queensland, Australia*; European Commission: Brussels, Belgium, 2022.
43. *Rihmond Valley Council Richmond Valley Flood 2022*; European Commission: Brussels, Belgium, 2022.
44. QUInewsPisa Incendio Fra Gli Olivi, Indagano i Carabinieri. Available online: https://www.quinewspisa.it/vicopisano-incendio-monte-pisano-olivi-indagano-carabinieri.htm (accessed on 20 December 2022).
45. EMS EMSR316: Forest Fire in Tuscany, Italy. Available online: https://emergency.copernicus.eu/mapping/list-of-components/EMSR316 (accessed on 20 December 2022).
46. EMS, C. Copernicus Emergency Management Service Monitors the Impact of Forest Fires in Portugal. Available online: https://emergency.copernicus.eu/mapping/ems/copernicus-emergency-management-service-monitors-impact-forest-fires-portugal (accessed on 20 December 2022).
47. Aguiar, F.C.; Rodrigues, C.; Pina, J.P.; Soares, P. Regeneration of Riparian and Maritime Pine Forests after a Large Wildfire on the Largest Public Forest of Portugal. *Forests* **2021**, *12*, 477. [CrossRef]
48. EMS EMSR250: Forest Fire Portugal. Available online: https://emergency.copernicus.eu/mapping/list-of-components/EMSR250/ALL/EMSR250_01MARINHAGRANDE (accessed on 20 December 2022).
49. CAL FIRE. 2020 Fire Season. Available online: https://www.fire.ca.gov/incidents/2020/ (accessed on 20 December 2022).
50. USDA Forest Service. *Burned-Area Report Nortx Complex*; USDA: Washington, DC, USA, 2020.
51. California Department of Forestry and Fire Protection California Fire Perimeters (All). Available online: https://gis.data.ca.gov/datasets/CALFIRE-Forestry::california-fire-perimeters-all-1/about (accessed on 20 December 2022).
52. USGS Earth Explorer. Available online: https://earthexplorer.usgs.gov/ (accessed on 12 November 2020).
53. ESA. Copernicus Open Access Hub. Available online: https://scihub.copernicus.eu/dhus/ (accessed on 11 December 2020).
54. JAXA ALOS Global Digital Surface Model “ALOS World 3D—30m (AW3D30)”. Available online: https://www.eorc.jaxa.jp/ALOS/en/dataset/aw3d30/aw3d30_e.htm (accessed on 18 January 2023).
55. ESA SNAP Download. Available online: https://step.esa.int/main/download/snap-download/ (accessed on 18 January 2023).
56. Congalton, R.G.; Jones, R.; Schrie, J. Evaluating Remotely Sensed Techniques for Mapping Riparian Vegetation. *Comput. Electron. Agric.* **2002**, *37*, 113–126. [CrossRef]
57. Matthews, B.W. Comparison of the Predicted and Observed Secondary Structure of T4 Phage Lysozyme. *Biochim. Biophys. Acta (BBA) Protein Struct.* **1975**, *405*, 442–451. [CrossRef]
58. Chicco, D.; Jurman, G. The Advantages of the Matthews Correlation Coefficient (MCC) over F1 Score and Accuracy in Binary Classification Evaluation. *BMC Genom.* **2020**, *21*, 6. [CrossRef]
59. Pereira, J.M.C.; Sá, A.C.L.; Sousa, A.M.O.; Silva, J.M.N.; Santos, T.N.; Carreiras, J.M.B. Remote Sensing of Large Wildfires. In *Remote Sensing of Large Wildfires*; Chuvieco, E., Ed.; Springer: Berlin/Heidelberg, Germany, 1999; ISBN 9783642601644.
60. Pinhal do Rei Incêndio de Agosto de 2003. Available online: https://pinhaldorei.net/historias-personagens/incendio-de-agosto-de-2003/ (accessed on 20 December 2022).